Compressible fluid model for hydrodynamic lubrication cavitation

G. Bayada
I.C.J. UMR CNRS 5208
INSA de Lyon
Bat. Léonard de Vinci

69621 Villeurbanne Cedex

guy.bayada@insa-lyon.fr

L. Chupin
Laboratoire de Mathématiques
Campus des Cezeaux
Univ. Blaise Pascal

63 177 Aubière Cedex

laurent.chupin@math.univ-bpclermont.fr

Keywords: cavitation, compressible Reynolds equation
Date: april 2013

Summary

In this paper, it is shown how vaporous cavitation in lubricant films can be modelled in a physically justified manner through the constitutive (compressibility) relation of the fluid. It is shown how the widely used Jakobsson-Floberg-Olsson (J.F.O.) / Elrod-Adams (E.A.) mass flow conservation model, can be compared with this new model. Moreover the new model can incorporate the variation of the viscosity in the cavitation region and allows the pressure to fall below a cavitation pressure. Numerical computations show that discrepancy with J.F.O./E.A. is mostly associated with light loading condition, starved situation or viscosity effects.

1 Introduction

It will be shown in this paper how continuum methods in which the flow is treated as an homogeneous compressible mixture allow to recover the main features of the widely used Jakobsson-Floberg-Olsson (J.F.O.) / Elrod-Adams (E.A.) mass flow conservation model for cavitation by using a generalized compressible Reynolds equation as a thin film approximation model.

Cavitation is a phenomenon occurring in numerous lubricated devices, mostly in the regions of diverging contact geometry where sub-ambient pressures can exist, and implies some diphasic characteristics for the lubricant. As early as 1956, experiments have been conducted by Cole and Hughes [1] for various mechanisms which show the complexity of the phenomenon. Cavitation has also been discussed in 1961 in the book of Pinkus and Sternlicht [2] . In Zeidan and Vance [3], various distinct operating regimes were identified in squeeze

film dampers. Other experiments are reported in Braun and Hendricks [4] for steady-state journal bearings, Sun and Brewe [5] for submerged bearings or San Andres and Diaz [6] for open-end submerged dampers, Ku and Tichy [7] for submerged squeeze film dampers. An extended review by Braun and Hannon may be found in [8]. Various types of models have been proposed to deal with this phenomenon and can be classified roughly in two categories. In the first one, the main feature of the cavitation phenomenon is the appearance of two distinct areas: the cavitation region and the full film one. The second kind of model leads to a generalized Reynolds equation satisfied on the whole contact area similar to the one proposed by Zuber and Dougherty in [9] for a two-phase fluid with droplets flying inside the fluid or by Chamniprasart et al [10] for bubbly fluid.

Despite various physical meanings, the first category of models belongs to the free boundary problems: It is essentially based upon the computation of the free (unknown) boundary of the cavitation area (Dowson Taylor [11]). The Reynolds or Swift-Stieber boundary condition associated with the Christopherson [12] algorithm has been widely used although it is not a mass flow conservative model. Jakobsson-Floberg-Olsson (J.F.O.) [13] type models are essentially mass conserving. One of the most popular algorithms to deal with this model is the Elrod-Adams (E.A.) [14] cavitation algorithm. In this pioneering article, a new formulation of the original JFO model is first addressed by introducing the fractional film content in the cavitation area. In a second step, introduction of a compressibility parameter in the non cavitated area and of a switch function allows to reformulate the problem in terms of a new variable. This variable satisfies a unique equation and has different interpretations in each of the subregions. This approach allows easier computation than the earlier JFO model.
Improvements of this algorithm have been proposed by Vijayaraghavan and Keith [15] and Brewe [16]. An equivalent “flow model” was used in Hirayama, Sakurai and Yabe [17] (following an idea of Ikeuchi and Mori [18] in which both density and viscosity vary, retaining the basic ideas of the Elrod-Adams algorithm). Other procedures have been proposed by Tichy [7], Bayada, Chambat and Elalaoui [19], Kumar and Booker [20] or Hajjam and Bonneau [21]. They solve the JFO model retaining the two unknowns formulation (pressure and fractional film content) of J.F.O./E.A. model without introducing the compressibility effects of the Elrod Adams algorithm.

It should be noted in these previous models that the pressure must be constant in the cavitated area and never falls below the cavitation pressure. However, sub-ambient pressure loop have been observed as early as 1982 by Etsion and Ludwig [22] and Braun and Hendricks [4] one year later. Values of pressure as small as 0.07 MPa. have been observed. At least two models overcome this deficiency and allow a small sub ambient pressure loop upstream of the point of separation: the flow separation model (Dowson and Taylor [11]) and the Coyne and Elrod model [23,24]. However these models have been described for 2-dimensional geometry (infinitely long devices, one dimensional Reynolds equation). They are not extended in their known form to a 3-D geometry. A model of dynamic cavitation incorporating surface tension and contact angle for parallel plate oscillatory squeeze film bearing has been proposed by Sun et al [25]. This model used the axisymmetrical assumption: A one-dimensional Reynolds equation is used together with an ordinary differential equation describing the evolution of the cavitation bubble. The model preserves mass conservation in the cavitation region and allows the occurrence of tensile stresses in the film. The role of the surface tension and contact angle is incorporated in the model. Geike and Popov [26] roughly follow the same idea. Numerical results show good agreement with those of Bodeo and Booker [27]. Two other descriptions of the cavitation using a free boundary approach have been proposed by Grooper and Etsion [28,29]. In the first paper, the effect of the shear of the cavity bubble by

the lubricant and of the gas diffusion through the interface is investigated while in the second paper the reverse flow phenomenon is included in the model: A reverse flow front develops in the full film region at the cavitation end, penetrates the cavitation and withdraws backward into the cavitation bubble. Compared with experiments, numerical results show that the reverse mechanism is capable of generating more realistic pressure than the first model mentioned. Let us mention also the work of Pan, Kim and Rencis [30] based on a reinterpretation of experimental photographic data which is however limited to an infinitely long device: The model stipulates a 3-D flow structure for transition from the filled fluid film to a cross-void fluid transportation process. The transition starts as a two-component composite rupture front and becomes an adherent film.
Note that another limitation using the free boundary approach like the J.F.O. model is the computation of the friction force in the cavitation area as information in this zone only concerns the pressure.

In the second category of models, the existence of a macro-bubble of cavitation is not assumed “a priori”. Cavitation is deduced from the solution of the constitutive equations of the lubricants so that a better knowledge of the characteristics of the mixture is necessary. Numerous papers have been devoted to this goal such as the one of Feng and Hahn [31]. Chamniprart et al [10] extended hydrodynamic lubrication theory to lubrication with mixtures. In this paper, a system of Reynolds like equation equations is obtained. Both relative gas bubble size and inlet air fraction are taken into account. Tao et al [32] proposed a continuum model describing the motion of a bubbly fluid in an open ended squeeze film damper. Bubbles of perfect gas are dispersed in an incompressible fluid with equal velocity. An isothermal process is assumed. They obtained a simpler thin film flow equation which is nothing else than a compressible Reynolds equation with an hyperbolic density-pressure law. Later on, Diaz and San Andres [33] used the same Reynolds equation with simpler viscosity-pressure law to study squeeze film dampers operating with bubbly fluids. Comparisons of predictions and test results show a relatively good correlation. Discrepancy is attributed to the existence of a large bubble which disrupts the mixture homogeneity.
More recently Xing, Braun and Li [34,35] used a full Navier-Stokes model with variable density and viscosity due to the change of void fraction (gaseous cavitation). Comparisons are made with both the Reynolds classical solution (without cavitation or with half Sommerfeld model) and with experiments. Van Odyck and Venner [36] also used a compressible Navier-Stokes system. They used a multigrid code and compared the solution of the Navier-Stokes equations with the one of Elrod-Adams. The results seem to demonstrate some limitations of the validity of the Reynolds compressible equation.
Finally it is possible to use some commercial codes such as Fluent or CFX to compute cavitating flows. In these codes and more generally in fluid mechanics [37], the fluid is assumed to be a mixture of liquid, vapour and non-condensable gases. Navier Stokes equation and continuity equations are written for the density. An additional transport equation for the vapor phase takes into account mass transfer between vapor and liquid. Mass fraction of non-condensable gas is a given constant. Evolution of the radius of the bubbles is often computed from the Rayleigh-Plesset equation to define mass transfer terms.
To summarize this introduction, it can be said that there are two types of approaches to model cavitation: On one hand, models based on a separation between a cavitated and a full film region, and on the other hand models in which a detailed description of the flow at a mixture level is needed. It will be shown how J.F.O./E.A. model can be derived from such Navier-Stokes flow detailed description.

2 Theory

Let us consider as a starting point the compressible Navier-Stokes equations with variable density and (dynamic) viscosity. We will show how is it possible to gain a thin film approximation which retains simultaneously both usual compressibility effects due to high pressures and phase transition. The model assumes that the lubricant can be described in an unified manner in both cavitated and non cavitated regions as an "equivalent" homogeneous compressible fluid. So, we will not be able to see "the details" of what happens in the real cavitation region. In its present form, non condensable gaz region is neglected so that only the vaporous cavitation is considered. It will be shown however that it allows to recover much of the properties of the J.F.O./E.A. model, improving it in some aspects. What we will denote by "cavitation region" will be the area in which the local density is less than the density of the liquid and greater than that of the vapour. In other words, the cavitation region will be a region of mixture.
In nearly all of the previous cited works, thermal effects are assumed to be negligible in the description of the cavitation model and a three dimensional energy equation is not considered. It can be taken into account in a second step by making coefficients of Reynolds equation (4) as a function of both density and temperature and introducing simplified energy equation as in Durany et all [38] .
Continuity and momentum equations are:

$$\frac{\partial(\rho\, u_i)}{\partial t}+u_j\frac{\partial(\rho\, u_i)}{\partial x_j}=\rho\, f_i+\frac{\partial \sigma_{ij}}{\partial x_j} \quad (1)$$

$$\frac{\partial \rho}{\partial t}+\frac{\partial(\rho u_j)}{\partial x_j}=0 \quad (2)$$

$$with\ \sigma_{ij}=2\mu+(\lambda\varepsilon_{kk}-p)\,\delta_{ij} \quad (3)$$

In which u_i are the velocity components, p the pressure, μ the viscosity(dynamic), ρ the density, f the external forces and λ a Lamé coefficient.
For known functions p(ρ), λ(ρ) and μ(ρ) and convenient boundary conditions, the goal is to compute the pressure field (or equivalently the density) and the velocity field satisfying (1)-(2)-(3). There are several possibilities for the choice of λ: the value λ= -2μ/3 (Stokes assumption) is often used. However it is not true for a lot of fluid and the choice λ(ρ)=2(ρ μ'(ρ)–μ(ρ)) has been proposed in [39]. This choice together with other assumptions concerning the behaviour of p(ρ), dp/dρ , μ(ρ) , dμ/dρ for large and small values of ρ allows to prove the well posedness of the system (1)(2)(3) in [39].

To obtain a thin film approximation of equations (1)-(2)-(3) is not obvious. It has been pointed out by Bair, Khonsari and Winer [40] that *the "fact of reintroducing some compressibility aspects in the Reynolds equation after some non dimensionalization and simplification, starting from incompressible Reynolds equation can be logically questioned*". It has been recently rigorously proven by Chupin and Sart [41] that the narrow gap approximation of the Navier-Stokes compressible equation (1)-(2)-(3) is exactly the "usual" compressible Reynolds equation. In some sense, this work is a mathematical proof and a generalization to compressible flows of an already proposed process in [42] and [43] for variable viscosity thin film flow.

Such a Reynolds equation is written down for a model device with a small gap $h(x_1,x_2)$ in which the upper part is fixed and the flat lower part has a constant velocity u along the x_1-main direction (see figure1).

$$\frac{\partial}{\partial x_1}\left(\frac{h^3}{12\mu(\rho)}G(\rho)\frac{\partial \rho}{\partial x_1}\right)+\frac{\partial}{\partial x_2}\left(\frac{h^3}{12\mu(\rho)}G(\rho)\frac{\partial \rho}{\partial x_2}\right)=u/2\,\frac{\partial(\rho h)}{\partial x_1}+\frac{\partial(\rho h)}{\partial t} \tag{4}$$

$$\text{with} \qquad G(\rho)=\rho\frac{dp}{d\rho} \tag{5}$$

Using the known one to one pressure-density relation, it is also possible to consider as unknown the pressure instead of the pressure by a simple change of function in the Reynolds equation (4). This expression is more convenient for comparison with previous cavitation models like the JFO/EA models .

$$\frac{\partial}{\partial x_1}\left(\frac{h^3}{12\mu(p)}(\rho(p)\frac{\partial p}{\partial x_1})\right)+\frac{\partial}{\partial x_2}\left(\frac{h^3}{12\mu(p)}(\rho(p)\frac{\partial p}{\partial x_2})\right)=u/2\,\frac{\partial(\rho(p)h)}{\partial x_1}+\frac{\partial(\rho(p)h)}{\partial t} \tag{6}$$

a) pressure-density relation

We choose a model based upon an isentropic assumption (7) which seems to be well adapted to the vaporous cavitation and is already widely used for cavitating flow([44],[45],[46]):

$$\frac{dp}{d\rho}=c_f^2 \tag{7}$$

in which c_f is the speed of sound in the medium. Equation (7) must be integrated to compute the pressure-density relation which it is necessary to know explicitly to solve equation (5).
In the context of a simplified model for the vaporous cavitation, we are led to consider 3 distinct regimes, one of mixture A_m, one of pure vapour A_v and one of pure liquid A_l . Coexistence of these 3 regimes implies physically a non-constant temperature. It has to be mentioned however that numerous experimental works as the recent one of Cristea, Bouyer, Fillon and Pascovici [47] show the existence of some temperature gradients, nevertheless small in cavitated bearings. This fact supports the possibility for the present theory in which the energy equation is neglected.

Let P_{vm} be the upper limit value of the pressure in A_v (also called the wet point) and P_{ml} the lower limit of the pressure in A_l (also called the bubble point). At a given temperature, this velocity is assumed to be a known constant for each of the regimes A_v and A_l , says c_v and c_l. In the mixture regime the sound velocity varies with the density ρ. Let us consider the void fraction α (Volume of vapour/volume total) . We have:

$$\alpha=(\rho-\rho_l)/(\rho_v-\rho_l) \tag{8a}$$

Or equivalently:

$$\rho(\alpha)=(1-\alpha)\,\rho_l+\alpha\,\rho_v \tag{8b}$$

in which ρ_v and ρ_l are the density of the vapour and of the liquid at the wet point and the bubble point respectively so that $0<\alpha<1$ as soon as $\rho_v<\rho<\rho_l$.

It is possible to use equation (8a) to generalize the definition of α for $\rho_v>\rho$ and $\rho>\rho_l$. Thus α could be less than 0 in A_l (compressibility case if $\rho>\rho_l$) or greater than 1 in A_v (rarefying situation if $\rho_v>\rho$). In these last cases, the initial definition of α as the volume fraction of the vapour is no longer valid. Symbol α will be retained to avoid introduction of additional notation.

Various models have been proposed for computing the velocity in the mixture region. In the sequel the relation proposed in Moreau [46] or Van Wijngaarden [48] will be used:

$$\frac{1}{c_f^2}=\rho\left(\frac{\alpha}{c_v^2\rho_v}+\frac{1-\alpha}{c_l^2\rho_l}\right) \qquad (9)$$

In this model, surface tension and mass transfer between vapour and liquid are neglected. It allows easy computation of the pressure-density law as follows:

The first step to gain this pressure-density law is to integrate equation (7) with respect to ρ in each of the 3 regions A_m, A_l and A_v using the expression (8) in A_m, so introducing 3 unknowns (The 3 constants of integration). Then taking into account that p(0)=0, the continuity of the pressure and of the derivative of the pressure for $\rho=\rho_v$ and for $\rho=\rho_l$, a system of 5 equations is obtained . The 5 unknowns: P_{vm} and P_{ml} (which will be also denoted P_{sat}) and the 3 constants of integration can now be calculated to obtain:

$$P_{vm}=\rho_v c_v^2 \quad (10a)$$

$$P_{ml}=\rho_v c_v^2-N\log\left(\frac{\rho_v^2 c_v^2}{\rho_l^2 c_l^2}\right) \quad (10b)$$

$$\text{with } N=\frac{\rho_v c_v^2\rho_l c_l^2(\rho_v-\rho_l)}{\rho_v^2 c_v^2-\rho_l^2 c_l^2} \quad (10c)$$

$$p(\alpha)=c_v^2\rho(\alpha) \quad if\ \alpha>1 \quad (11a)$$

$$p(\alpha)=P_{ml}+(\rho(\alpha)-\rho_l)c_l^2 \quad if\ \alpha<0 \quad (11b)$$

$$p(\alpha)=P_{ml}+N\log\left(\frac{\rho_v c_v^2\rho(\alpha)}{\rho_l(\rho_v c_v^2(1-\alpha)+\rho_l c_l^2\alpha)}\right) \quad if\ 0<\alpha<1 \quad (12)$$

Equations (10)-(11)-(12) allow to compute the pressure –density relation as soon as the values of the velocity of the sound and the density are known for each of the pure regimes at a given temperature An example of such a pressure-density function obtained from equations (10)-(11) is given in Figures 2 and 3. Discussion about the influence of these coefficients on the solution of the equations (4)(5)(6) will take place in section 4.

b) viscosity-density relation in the mixture

There exists various formulae to obtain the viscosity of a mixture [49,50,51,52] from the known values in the pure regimes μ_l and μ_v at a given temperature. In the following, we choose to use two of them which have been recently put forward in [34] and in [53] in the lubrication area:

$$\mu(\alpha)=\alpha\mu_v+(1-\alpha)\mu_l \quad \textit{Dukler assumption} \quad (13)$$

$$1/\mu(\alpha)=M(\alpha)/\mu_v+(1-M(\alpha))/\mu_l \quad \textit{McAdams assumption} \quad (14)$$

In which M is the mass fraction of the vapour defined for $0<\alpha<1$ by:

$$M(\alpha)=\alpha\frac{\rho_v}{\rho(\alpha)} \qquad (15)$$

To be noted also that these formulae are valid for a mixture of vapor –liquid from the same fluid and not from a mixture of two different fluids for which another laws must be used.
The previous Reynolds equations (4)-(5) can also be written down in dimensionless form by making the change of variable (8b). This can be more convenient for computation as α as a limited range.
Let l be the characteristic length in the cross film direction, L_1 in the main direction of the device, L_2 in the axial direction,V a characteristic value of the velocity, see Figure 1. Let us introduce :

$$H = h/l, \quad X_1 = x_1/L_1, \quad X_2 = x_2/L_2, \quad S = u/V, \quad \rho^* = \rho/\rho_l, \quad t^* = t\,V/L_1$$
$$\mu^* = \mu/\mu_l, \quad p^* = pL_1^2/L_2V\mu_l \quad r_c = c_v/c_l, \quad r_\rho = \rho_v/\rho_l, \quad r_\mu = \mu_v/\mu_l,$$

and the dimensionless modified Reynolds number:

$$\Re=(lc_l)^2\rho_l/(L_1V\mu_l)$$

Performing the change of variable defined by equation (8), using equations 11(a),11(b),(12) to compute G(ρ) in (6) in terms of α ,the Reynolds compressible equation (5) can be rewritten as:

$$(r_\rho-1)\,\Re\left[\frac{\partial}{\partial X_1}\left(H^3(X)\frac{Q(\alpha)}{12\,\mu^*(\alpha)}\frac{\partial\alpha}{\partial X_1}\right)+(L_1/L_2)^2\frac{\partial}{\partial X_2}\left(H^3(X)\frac{Q(\alpha)}{12\,\mu^*(\alpha)}\frac{\partial\alpha}{\partial X_2}\right)\right]=$$
$$\frac{\partial}{\partial t^*}(H(X)(\alpha\,r_\rho+(1-\alpha))) \quad (16)$$
$$-\frac{1}{2}S\frac{\partial}{\partial X_1}(H(X)\,(\alpha\,r_\rho+(1-\alpha))+\textit{with}$$
$$Q(\alpha)=(1-\alpha)+\alpha\,r_\rho \quad \textit{if} \quad \alpha<0; \quad (17)$$
$$Q(\alpha)=1/\left((1-\alpha)+\frac{\alpha}{r_\rho r_c^2}\right) \textit{ if } 0<\alpha<1 \quad (18)$$
$$Q(\alpha)=r_c^2((1-\alpha)+\alpha\,r_\rho) \textit{ if } \alpha>1 \quad (19)$$

It should be noted that the dimensionless number $\Re$ only relies on rheological values of the liquid phase while Q only depends on the ratio of the pure vapour and pure liquid density and speed of sound. Moreover the pressure density law (10)-(11)-(12) is implicitly included in the coefficients with Q(α).

Let us remark that the present model can give an approximate value for the bulk modulus β used in the Elrod-Adams algorithm ([14],page 39) (see the following section for more comments): The bulk modulus β is such that:

$$p=P_{cav}+\beta \log(\frac{\rho}{\rho_c})=P_{cav}+\beta \log(1+\frac{\rho-\rho_c}{\rho_c})\simeq \qquad (20)$$

At the beginning of the non cavitated area, ρ is close to ρ_c so that the last portion of equation (20) can be approximated by $P_{cav}+\beta(\rho-\rho_c)/\rho$.

This can be compared with equation (11b). As P_{cav} and ρ_c in [14] have the same meaning than P_{ml} and ρ_l in section 2 , so they are identical and we get:

$$\beta \simeq \approx \rho_l \ c_l^2 \qquad (21)$$

3 Comparison of compressibility laws

In this section, we compare the compressibility law of the present theory defined by equations (10)-(11)-(12) with some other laws which are used in the lubrication literature. Qualitative agreement with J.F.O. / E.A. model seems to be good, supporting the fact that compressibility effects are the basic ingredient for J.F.O. like cavitation models.

In this pioneering paper [14], Elrod and Adams firstly gave a new formulation of the initial J.F.O. model in which the cavitation is associated with a function θ (such that $0\leq\theta\leq 1$) used to describe the "mass flow in the cavitated region"(Floberg's hypothesis). Then, they applied the usual (pressure-density) relation in the full film region, assuming a constant bulk modulus β defined by (20) and defining θ in this region as the ratio ρ/ρ_c.
They retained the assumption of constant pressure ($p=P_{cav}$) in the cavitation area defined by ($\rho<\rho_c$) and the condition $p>P_{cav}$ in the full film area defined by ($\rho>\rho_c$). The related equation is assumed to be easier to solve than the one in the J.F.O. model
Although not mentioned in the text, the proposed model described by equation (15) in [14] can be also viewed as a compressible Reynolds equation with constant viscosity and a pressure compressibility law as the one in Figure 1 (see also Figure 2 of [13]) .
The choice β=0.069 GPa in [14] was not discussed in the paper. Computation with this value is easier than using higher values. It is however much smaller than the value obtained with equation (21) or predicted by various authors [54] which is around 2 GPa for water or oil. If the goal is to use E.A. to solve J.F.O. model which assumes incompressible materials, we must have to choose a higher value for β. Computation of the solution of equation (16) shows that β must be chosen as high as 1000 GPa to obtain a good approximation of the JFO solution if the pressure reaches 40 Mpa. Let us also remark that the original JFO model corresponds to a pressure-density law with straight horizontal part for $p>P_{cav}$ (infinite value for β).

Sahlin, Almquist, Larsson and Glavatskih [55] don't modify the whole Elrod-Adams strategy . They proposed to use the following Dowson and Higginson expression (22) which connects pressure and density [56]:

$$p=P_{cav}+C_1\frac{\rho_c-\rho}{\rho-\rho_c C_2} \qquad (22)$$

They use the original expression (C_1=0.59 10^9, C_2=1.34) instead of (20) or a modified one fitted to experimental data (C_1=2.29 10^9 , C_2=1.66) .
They showed how discrepancies appear between the pressure computed by their procedure and the solution to the E.A. model. They highlight the importance of the choice of the bulk modulus parameter.

A different pressure compressibility relation has been proposed by Van Odyck and Venner [36], based on the work of Dellannoy and Kueny [57] and of Hoeijmakers, Jansens and Kwan [58]for a two phase flow problem. For numerical computations, the viscosity is taken to be constant everywhere although a possible variation with respect to the pressure is mentioned. The pressure-density relationship is such that

$$\rho=\rho_v \quad for \quad p<P_{cav}-\Delta p \quad (23a)$$
$$\rho=\rho_l \quad for \quad p<P_{cav}+\Delta p \quad (23b)$$

while in the mixture they get:

$$\rho=\rho_v+\Delta\rho\,(1+\sin(\frac{p-P_{cav}}{\Delta\rho\; c^2_{\min}})) \quad (24a)$$
$$with \quad \Delta\rho=1/2\,(\rho_l-\rho_v) \quad (24b)$$
$$\Delta p=1/2\;\pi\;\Delta\rho \quad (24c)$$
$$and \quad c^2_{\min}=2c_v\sqrt{\frac{\rho_v}{\rho_l}} \quad (24d)$$

A comparison for these various compressibility laws is given in fig (2)-(3).
For the present model, the data used are:

$$\rho_v=1\ kg/m^3 \quad \rho_l=998\ kg/m^3 \quad c_v=343\ m/s \quad c_l=1480\ m/s$$

The bulk modulus used for E.A model is the one given by equation (21), let β=2.2 GPa. It is clear from fig (2) that the density-pressure curves defined by (11)-(12) and (23)-(24) are globally very closed. How to choose P_{cav} is not specified in [36]. It has been arbitrarily fixed in (Fig 2) as $P_{cav} = (P_{vm}+P_{ml})/2$. However another choice like $P_{cav} = P_{ml}$ could give a better correlation in the transition zone. Some discrepancies occur for high pressure values as compressibility effects are ignored in (23)-(24).
Let us mention also that if the values of c_l and ρ_l can be relatively easily known [46], this is not the case for c_v and ρ_v . As it will be seen in section 4, changing the values of c_v and ρ_v induces changes in $P_{ml.}$ This does not modify however the overall shape of the pressure-density relation. Choosing for P_{cav} in (23)-(24) or in E.A. model the same value as P_{ml} maintains a good correlation between the various models.
For higher pressure, the present model is very close to the E.A. one up to 0.3 GPa while some discrepancies appear with both Dowson-Higginson (Do.Hi.) model, especially with the modified one.

4 Numerical results. A first comparative case.
Equations (4)-(6) have been written down for a 3-dimensional device in unsteady situation. If the gap does not depend on the time and if boundary conditions are constant in time, the solution of this equation tends to a function which does not rely on time and satisfies the steady state Reynolds equation. From now on, for comparison with other authors for which the pressure is the main unknown, steady state solution of (6) will be computed.

As a first comparative test case, the parabolic slider (the infinitely long device assumption with the notation x instead of x_1) already proposed by Vijayaraghavan and Keith [15] and Sahlin and coauthors [54] is used. Comparisons between the present compressible model ,

Elrod-Adams (E.A.) model, Dowson-Higginson (Do.Hi.) model for various bulk modulus and cavitation pressure are given. In this situation (moderate loading, fully flooded situation), the coincidence of these various models with the present one is remarkable, both for the pressure p and "saturation" or relative density ρ/ρ_l (Figures 5 and 6). The main difference is the existence of some "under-pressure" in the cavitated area with the present model.

For the infinitely long device, it is not necessary to solve the Reynolds equation (6) using a finite difference or finite element method as for a finite dimensional device (see section 9). The second term of the left hand side of the Reynolds compressible equation (6) disappears. (the same procedure can be used for equation (16)). The Reynolds equation becomes an ordinary differential equation of second order (notation x_1 is replaced by x). This equation is equivalent to a system of two first order differential equations:

$$\frac{dQ}{dx}=0 \quad (25a)$$

$$Q=-\frac{h(x)^3\rho}{12\mu}\frac{dp}{dx}+\frac{\rho h(x)u}{2} \quad (25b)$$

with the boundary conditions:

$$p(x=0)=p(x=L)=P_{ext}=10^5 \text{ Pa} \quad (25c)$$

As boundary conditions are imposed on the pressure the value of the input mass flow Q is not known. It is is computed by the following procedure:
The ordinary differential equation (25b) is solved using a shooting method: the pressure boundary condition is applied at one of the boundary namely x=L and the value of the input mass flow Q is adjusted so that the other boundary condition at x=0 is satisfied. Usual algorithms like Runge-Kutta 4 with 5000 nodes are used.

From the knowledge of p (or equivalently ρ or α), it is easy to compute the (relative) density ρ/ρ_l, the friction F on the moving surface and the load W:

$$F=\int_0^L\left(-\frac{\mu(x)\rho(x)u}{h(x)}-\frac{h(x)}{2}\frac{dp}{dx}\right)dx, \quad W=\int_0^L(p-P_{ext})\,dx \quad (26)$$

It should be noticed that the formula used for the computation of the friction is valid on the whole surface of the device and no assumption has to be made on the value of the friction over the cavitated area.

Both Elrod-Adams and Dowson-Higginson model used a dimensionless density which is given by the ratio ρ/ρ_l in the non cavitated area and "local proportion" of fluid θ in the cavitation area. It can be compared with the ratio ρ/ρ_l of the present model (figure 6) and its minimum value is given in column 4 of Table 1.

Data are [55]: (Figure 4)

$u= 4.57$ m/s $\quad 0<x< L=0.0762$ m $\quad \mu_l= 0.039$ Pa.s

$h_{max}= 5.08\ 10^{-5}$ m $\quad h_{min}=2.54\ 10^{-5}$ m

The present model is associated with the following additional fluid properties (The influence of the values of these parameters will be studied in the next section):

$\rho_l=950$ kg/m^3 $\quad c_l= 1600$ m/s $\quad r_\rho=2\ 10^{-5}$ $\quad r_\mu=0.017$ $\quad r_c=0.22$

Operational parameters for the various models are given in Table 1. The first row gives the result obtained using the E.A. algorithm with the value of β used in [13,14]. In the second row the value of β deduced from Equation (21) is used. The two following rows are concerned with the Dowson-Higginson. model of compressibility and the data issued from [55]. Two different values of the saturation pressure 1 bar (as in [55]) or 0.6 bar are used. The last one is exactly the pressure P_{ml} deduced from equation (10) using the previous choice for ρ_l, c_l, r_ρ, r_c. For the last row which is concerned with the present model, both Dukler and McAdams mixture viscosity models give the same values.

The two values for the friction mentioned for each row are obtained for the first figure by the computation of:

$$-\int_{\grave{a}}^{L} h\frac{dp}{dx}dx-\int_{0}^{L}\frac{u\mu}{h}dx \qquad (27)$$

This is the classical formula, assuming it is valid on the whole surface of the device , including the cavitation area.
For the second figure zero friction in assumed in the cavitated area so that friction is computed by:

$$-\int_{\grave{a}}^{L} h\frac{dp}{dx}dx-\int_{0}^{L}\frac{u\mu}{h}\Psi(p)dx \quad (28a)$$

with

$$\Psi(p)=1 \ if \ p>Pcav \ \text{ and } \ \Psi(p)=0 \ if \ p<Pcav \quad (28b)$$

For the present model, the friction is computed directly from (26) as the theory is valid uniformly in the whole domain so that only one figure is given.

The discrepancy between the two first rows in Table 1 has already been observed by Sahlin and co-authors as the good correlation with the Do.Hi. model. The relative density reaches 1.08 (Figure 6) for β= 0.069 GPa as a consequence of a too small value of the bulk modulus. For all other computations the relative saturation does not not exceed 1.001 so supporting the fact that incompressibility is reached. Concerning the friction, these results clearly show that it must be computed on the whole surface of the device and not only on the non cavitated area if J.F.O. or Do.Hi. models are used.
With the exception of the case β=0.069 GPa, the coincidence of all pressure and saturation curves in the non cavitated area is remarkable (most of the curves are superimposed in Figures 5 and 6). Consequences of a change of the cavitation value are mainly limited to the behaviour of the pressure in the cavitation area.
A close examination of the pressure curve (Figure 5) for the present model shows that the minimum value of the pressure is around 0.3 bar, less than saturation pressure P_{ml}.

5 Effects of the mixture viscosity model and vapor/liquid properties: A parametric study.

Physical parameters describing the properties of lubricant in the pure liquid and in pure vapour situations can cover a wide range of values [59]. In this section, a lot of computations have been conducted, for various parameters r_ρ, r_μ and r_c. The choice of the range of

parameters for the computations has been done so that changes of behaviour appear in the results in Tables 2 to 5. The computed load and the minimal value of the relative saturation are given in Tables 2, 3 and 4.
To make the discussion clearer, we choose to present the results in real dimensional variables starting from a fluid with ρ_l=950 kg/m^3 , μ_l= 0.039 Pa.s and c_l=1600 m/s. Geometrical data and velocity are the same as in section 4. Other values could not change quantitatively the results. As mentioned before, after suitable dimensionless procedure, only the ratio of viscosities, velocities and density are of interest, see Equation (16), so that these 3 parameters will be considered. Moreover results with Dukler and Mc Adams assumptions are compared**.**

The main feature in all tables and for both models is that results are nearly identical with the exception of a sudden decrease of the load for large values of r_c and r_ρ.. This effect can be explained by computing the saturation pressure P_{ml} from equation (10b). The decrease of the load occurs when the pressure P_{ml} is greater than the inlet pressure (1 bar) so that a local non saturated area exists at the entrance of the device. If the difference between P_{ml} and P_{ext} is not large, the pressure can increase in this area and the effect of this non saturated area is negligible. If the difference becomes too large, the pressure cannot increase sufficiently and it is exactly as if starvation appears. This induces a dramatic decrease of the load. This behaviour is illustrated in Figures 7 and 8 which correspond to the row r_c=0.25 from Table 2. Pressure curves for r_ρ= 4 10^{-5} and r_ρ= 5 10^{-5} (respectively r_ρ= 7 10^{-5} and r_ρ= 8 10^{-5}) are superimposed. This is also the case for the density curves for r_ρ= 4 $10^{-5}$and r_ρ= 5 10^{-5}.

Let us now consider the influence of the mixture viscosity model. For $r_\mu > 10^{-2}$ results are the same for both mixture viscosity models (Table 2). However, when this ratio decreases, the behaviour of the two models is very different. The results with Dukler's model are the same for any value of r_μ while those using the Mc Adams model heavily relies on the r_μ ratio (Tables 3 and 4). To explain the difference between the two mixture viscosity models, it can be pointed out that for small r_ρ and r_μ values, Equations (13) and (14) can be approximated by

$$\mu \approx \mu_l (1-\alpha) \quad \text{Dukler model} \quad (29)$$

$$\mu \approx \frac{\mu_l}{\frac{\alpha}{1-\alpha}\frac{r_\rho}{r_\mu}+1} \quad \text{McAdams model} \quad (30)$$

Then for small values of the ratio r_ρ and r_μ, the mixture viscosity in the first model is nearly independent from r_μ and r_ρ. For the second model, the viscosity heavily depends on the ratio r_ρ/r_μ. For the values of α far from 1, the viscosity in the first model has the same order of magnitude than μ_l while for the Mc Adams model it can reach values much lower if r_ρ/r_μ is large.

As a conclusion, it seems from the present computation that the influence of the vapour/liquid parameters is mainly related to the vapour/liquid transition pressure and then to the possible appearance of starvation. In that case, the Mc Adams model amplifies the variation of pressure compared to the Dukler model.

6 Light loading

It has been seen in Section 4 that for moderately loaded bearing, the solution of the present is close to the solution of J.F.O. or E.A. models if the cavitation pressure in J.F.O. /E.A. model is specified equal to the P_{ml} value and the bulk modulus is chosen according to equation (21). It will be seen here that it is not the case for lightly loaded bearing for which large discrepancies can exist, depending on the values of the internal parameters and the choice of the mixture viscosity model.

The following input data are chosen in this section:

$$h_{max}= 10\text{-}4 \text{ m} \quad h_{min}= 0.8\ 10\text{-}4\text{m} \quad l =0.314 \quad s=5\text{m/s} \quad p_{ext}= 1 \text{ bar},$$

with the fluid characteristics:

$$\rho_l= 900 \text{ kg/m3} \qquad c_l=1450 \text{ m/s}.$$

The E.A. algorithm is used first to compute load, maximal pressure, and minimal saturation (Table 6). A value of β and a cavitation pressure are needed: The value of β computed from equation (21) is 1.89 GPa. Three values of P_{cav}: 0.08 bar, 0.37 bar and 0.91 bar are used, Results are given in Table 6.

Solution for the full compressible fluid model is computed for three situations. In each case, the parameters are chosen such that the pressure P_{ml} obtained from equation (10) is the same as the pressure P_{cav} used in the previous E.A. computation:

$r_\rho= 6\ 10\text{-}5$ and $r_c =0.05$ for $P_{cav} =0.08$ bar
$r_\rho = 8\ 10\text{-}5$ and $r_c = 0.1$ for $P_{cav} = 0.37$ bar
$r_\rho = 5\ 10\text{-}5$ and $r_c = 0.2$ for $P_{cav}=0.91$ bar

Moreover, both Dukler and Mac Adams models are considered with three values of r_μ: 10^{-4}, 10^5 and 10^{-6}. Results are summarized in Table 7.
The difference between the E.A solution and the one for the present model increases with P_{cav}. The main reason is that under-pressures allowed by the present model are more important if P_{cav} is large. Moreover, the difference for the maximal pressure is smaller than the one for the load. So it can be inferred that the difference is mainly due to what happens around the "cavitation area".
Solutions with the Mc Adams model for r_μ greater than 10^{-4} and with the Dukler model for any r_μ are close to the E.A. solution. The solutions with the Dukler model are always independent from r_μ (computations from $r_\mu=10^{-2}$ to $r_\mu=10^{-8}$ always give the same result) while pressure and load for the Mac Adams model decrease like r_μ. This kind of phenomenon has already been observed in Section 5.
For the present model, it can be observed in Figures 9 and 10 that the cavitation area (relative saturation less than 1) increases with P_{ml} and with the decrease of r_μ. Moreover, in this aera, the pressure is roughly equal to half of the saturation pressure P_{cav}. This explains the evolution of the load with P_{cav} and r_μ. It should be noted also that the increase of the cavitation area is linked with an increase of the relative saturation: For $P_{cav} =0.91$ bar and $r_\mu =10^{-6}$, half of the device cavitates, being however near full of fluid.
The computation of the friction using (26) shows that it is constant for all computation, independent from the model, from r_μ and P_{cav}.
As a conclusion, the choice of the mixture viscosity model is of primary importance. Comparing with the Mc Adams model, the assumption $p> P_{cav}$ included in the E.A. models

can lead to important errors (60%) for small r_μ ($r_\mu > 10^{-4}$) even with "optimal" choices for $P_{cav} = P_{ml}$ and β computed from (21).

7 Moderate loading

In the previous sections, we essentially focussed on what happens around the "cavitation region". In this section, we compare the E.A. and Do.Hi. solutions with that of the present model in a situation in which high pressures exist.

Let us consider now a twin parabolic slider (Figure 11) as in [55]. The upper surface combines 3 flat areas of length L_{11},L_{12}, L_{13} and two parabolas of length L_{31} and L_{32}. The gap for the flat surfaces is denoted h_{max} and the minimum gap h_{min}. It can allow both starvation and inter-asperity cavitation, assuming the validity of the present cavitation model on the whole surface of the device as it is a common practice for usual cavitation models. Let us recall that previous studies [60] demonstrate the sensitivity of the results with respect to the cavitation models for rough surfaces. This is due to the succession of rupture /reformation free boundaries appearing in this situation.
Following data is used:

$$r_\mu = 0.017 \quad r_c = 0.05 \quad r_\rho = 5\ 10^{-5} \quad \rho_l = 992 kg/m^3 \quad \mu_l = 60\ 10^{-5}\ Pa.s \quad c_l = 1450\ m/s$$

$$h_{min} = 10^{-6} m \quad h_{max} = 4\ 10^{-6}\ m \quad s = 8 m/s \quad L_{31} = L_{32} = 0.5 m \quad L_{11} = L_{12} = L_{13} = 0.1 m$$

The corresponding cavitation pressure is P_{cav} = 0.07 bar which is chosen for the E.A. model although at this level of pressure other choices like 0 or 1 bar do not induce any differences. Operational parameters values for the various models are given in Table 8.
The present model (both Mc Adams and Dukler assumptions give the same results) gives values very close to the one of the Do.Hi. model and of the E. A. one for $\beta = 2.2\ 10^9$ GPa. From the results of Table 8, the importance of the choice of β in the E.A. model is noteworthy: In this situation, it is necessary to choose β greater than 10^2 GPa to get the J.F.O. incompressible case while a choice smaller than the "optimal choice" β=2.2GPa computed from (21) induces a dramatic decrease of the load. This is the result of the elasticity of the fluid which becomes more and more incompressible as β increases.
The elasticity of the fluid linked to the compressibility properties is not the only property to take into account to discuss the results of Table(8). In figure(3), the pressure density curve for the present model is above the one of the Do-Hi model and the last one is also above those of the E.A. incompressible case ($\beta = 22\ 10^9$ GPa) which is superimposed with the horizontal line. We can then expect that pressure and load for the E.A incompressible case are higher than those of the Do-Hi case and of the present model. This is not what appears in Table 8. The explanation is that the cavitation areas for the various models are different as in figure (13). The percentage of the surface corresponding to the non cavitated area is given in the last column of Table (8). As a consequence the solution of the Reynolds equation for the E.A. incompressible case (3th or 4th row) is computed on a domain which is smaller than the one for the present model or the Do-Hi model . In spite of the compressibility effect , load and maximal pressure for the incompressible model are smaller than for the two other models.

8 Starvation

Starvation at the inlet is often related to the fact that inlet flows are incomplete due to the geometry of the supply device or an insufficient input mass flow value. It is often associated with mixed lubrication. However it can be introduced also in the case of pure hydrodynamic solution [61,62,63]. In the J.F.O. model as in the present one, it is easy to take into account input flow rate Q as a input data and so to study a starved situation. A decrease of this value induces a starvation at the inlet. In the following results (Table 9 and Figures 12), input flow rate is chosen as 4.84 10^{-6} m^2/s, smaller than all the flow rate values in Table 8. Three regions of cavitation can be observed. The first one at the entrance, the second one between the 2 asperities and the last one before the outlet.

It should first be noted that the results for the present model and the E.A. one with β=2.2 10^9 GPa are nearly identical and the curves are superimposed. Cavitation boundaries for these two models and the Dowson-Higginson one are nearly identical and the difference between these 3 models is very limited.

Contrary to the fully flooded case, and despite the fact that the cavitation regions are also different, the solutions for the various models are in accordance with the pressure density curves of figure (3).

As it appears from Table 9 and Figure 12, differences between the other models are larger than in the previous fully flooded situation. Comparing with Table (8), the most intriguing aspect is that the decrease of the load is very different according to the model. For the present model, the ratio of decrease is 74%, while for β= 2.2 10^{10} Pa it is 63% and for β= 2.2 10^{11} Pa it is only 14%. This is the consequence of the different values for Q in the fully flooded situation: The relative decrease of the input flow is much more important for β= 2.2 10^9 Pa than for β= 2.2 10^{11} Pa. This explains why the incompressible solution now becomes greater than other solutions, contrary to the fully flooded case. The combined sensitivity of the solution relative to the bulk parameter and the flow rate is then exacerbated. When pressure built up occurs from a cavitated region, the differences between the models are larger than in the fully flooded solution. Such behaviour has already been observed in [60] and [64] using classical cavitation models.

9 A 2-dimensional example.

An interesting feature of the present model is the possibility of using a very simple algorithm to obtain the solution of the Reynolds equation (16) without any specific process for maintain the pressure at a value higher than a one given as a data (cavitation pressure).

Starting from an initial value for α satisfying the given boundary conditions, a sequence (α_{n+1}) satisfying the (linear) problem is computed:

$$(r_\rho - 1)\,\Re\left[\frac{\partial}{\partial X_1}\left(H^3(x)\frac{Q(\alpha_n)}{12\mu^*(\alpha_n)}\frac{\partial \alpha_{n+1}}{\partial X_1}\right)+(L_1/L_2)^2\frac{\partial}{\partial X_2}\left(H^3(x)\frac{Q(\alpha_n)}{12\mu^*(\alpha_n)}\frac{\partial \alpha_{n+1}}{\partial X_2}\right)\right] \quad (31)$$
$$=\frac{1}{2}S\frac{\partial}{\partial X_1}\left(H(x)\;\left(\alpha_n r_\rho+(1-\alpha_n)\right)\right)$$

Solution of this linear problem can be made by using finite difference or finite elements discretization. As an example, let us consider (half) a journal bearing like the one studied in [47] in which both pressure and temperature maps have been obtained. The previous algorithm has been used with 120 000 triangles P1-finite elements.

Input data from [47] are:

length=0.02m Radius =0.05m Eccentricity (computed to get 500N load)=0.735
ρ_l=900Kg/m3 μ_l =0.03 Pa.s Supply pressure =2 bar

Boundary pressure for the open-side = 1 bar and the relative velocity = 5m/s.
Supplementary data are chosen as:

$$\rho_v=0.018,\ \mu_v=0.00003,\quad c_v=333\ m/s,\quad c_l=1450m/s$$

So that the value of the saturation pressure P_{ml} is 0.51 bar (Choice of other values of ρ_v and c_v leading to saturation values from 0.35 to 0.65 does not change the results).

Results (Figure 13 middle) are compared with the experimental results (Figure 13 top) of [47] and with the results of a finite difference computation with the J.F.O. model using the algorithm issued from [65] (Figure 13 bottom).
Obviously the three solutions are very close in the convergent part of the bearing. The maximum pressure is the same 12.5 /13 bar. In the divergent region, solutions of the J.F.O. model and of the present one are also very close. The improvement is that we are able with the new model to gain precise information on what happens in the mixture-cavitation region . The computed minimal pressure is 0.2 bar (0.3 bar below the saturation pressure), the same value than the experimental one. However, the mixture–cavitation area in the new model covers an important part of the surface (even if a saturation pressure of 0.3 bar is taken as input data) contrary to what appears from experimental measurements. Moreover the location of the minimal pressure (marked by a cross) is not located at the same place. A possible explanation relies on the values chosen for the supplementary data although as mentioned before a wide range of saturation pressure has been tested with only small variations for the results. A more plausible explanation is that the present model does not take into account the air which enters the bearing as the pressure in the divergent part is very low with regard to the external pressure. Other phenomena such as gas diffusion [28] out and back into the lubricant or the reverse flow [29] which have been observed even in submerged bearing could also have some influences in the extent of the cavitation area. At last thermal effects could also play a role to explain this difference.
However, influence of the air entrance in the bearing does not seem to be the leading phenomenon in this situation as the overall pressure repartition above saturation pressure is not modified. This gives confidence to use the present model or the J.F.O./E.A. model in practical situations.

10 Conclusion

Although the J.F.O./E.A. model is widely used, it has never been possible so far to give a three dimensional (Navier)-Stokes model such that J.F.O/E.A could be considered as its thin film counterpart.
It has been described how a film thin Reynolds equation retaining the main features of the J.F.O./E.A. model can be obtained from of a full compressible (Navier)-Stokes model The model assumes that the lubricant can be described in an unified manner in both cavitated and non cavitated regions as an “equivalent” homogeneous compressible fluid. No geometrical assumptions on the shape of the three dimensional cavitation region is required.

The present model can be considered also as an approximation of the J.F.O/E.A model by using a smooth pressure-density relation (or compressibility law) valid on the whole lubricated surface.
Moreover values of the parameters involved in the E.A algorithm like saturation pressure and bulk modulus can be precisely obtained.
The possible appearance of 'negative pressure" (subcavitation pressure) is naturally included in the present model together with the variation of the viscosity. This is the main difference with the usual JFO/E.A. model which can become of importance especially for light loading situations. The choice of the viscosity model in the mixture can impact the performances of the devices.
The unified treatment of the cavitating and non cavitating regions of the flow shows that it is not necessary to consider a specific algorithm to cope with the cavitation. Usual algorithms can be used.

11 Acknowledgement

Thanks to professor Michel Lance of Laboratoire Mecanique des Fluides et Acoustiques, CNRS , Ecole Centrale de Lyon for various interesting discussions and to the referees for their valuable and numerous suggestions to improve the manuscript.

References

[1] Cole, J.A. and Hughes,C.J., 1956,"Oil flow and film extend in complete Journal bearings,"Proc. ImechE (170), pp 499-510.

[2] Pinkus ,O. and Sternlicht, B.: Theory of Hydrodynamic lubrication,Mc Graw –Hill Book Co. 1961, New York.

[3] Zeiden, F.Y. and Vance, J.M. , 1990, " Cavitation regimes in Squeeze Film Dampers and their Effect on the pressure distribution," Tribology Transactions 33(3), pp. 447-453.

[4] Braun , M.J. and Hendricks, R.C., 1983, " An experimental Investigation of the Vaporous/Gaseous Cavity Characteristics of an Eccentric Journal Bearing,"ASLE Trans., 27, 1, pp.1-14.

[5] Sun, D.C, Brewe, D.E. and Abel, P.B., 1993,"Simultaneous Pressure Measurement and High –Speed Photography Study of Cavitation in a Dynamically loaded Journal Bearing," ASME J. Trib., 115, pp. 88-95.

[6] Diaz, S. and San Andrés, L.A., 2001," A model for Squeeze film Dampers Operating with Air Entrainment and Validation With Experiments," ASME J. Trib, 123,pp. 125-133.

[7] Ku, C-P and Tichy, J.,1990 ," An experimental and Theoritical Study of Cavitation in a Finite Submerged Squeeze Film Damper," ASME J. Tribology, 112,pp. 25-733.

[8] Braun,M.J. and Hannon, W.M., 2010,"Cavitation formation and modelling for fluid film bearings: A review, "Proc. Imech. 224, Part J : J. Eng. Tribology, pp. 939-863.

[9] Zuber N. and Dougherty D.E., 1982,"The field equations for two phase Reynolds film flow with a change of phase, "ASLE Transactions, 25(1), pp. 108-116.

[10] Dowson, D. and Taylor, C.M.,1975," Fundamental aspects of cavitation in bearings," in *Cavitation and related phenomena in lubrication*, Mechanical Engineering Publications for the Institute of Tribology, The University of Leeds, pp. 15-25.

[11] Christopherson, D.G.,1941," A new mathematical method for the solution of film lubrication problem," Inst. Mech. Eng. Proc. 146, pp.126-135.

[12] Jakobsson, B. and Floberg, L. ,1957, " The finite journal bearing considering vaporization", Transactions of the Chalmers Univ. Technology, Gothenburg, 190.

[13] Elrod, H.G. and Adams, L., 1975,"A Computer program for Cavitation and Starvation," *in Cavitation and related phenomena in lubrication*, Mechanical Engineering Publications for the Institute of Tribology, The University of Leeds, pp. 37-41.

[14] Vijayaraghavan, D and Keith, Jr, T.G. ,1990, " An efficient, robust and time accurate Numerical Scheme applied to a cavitation algorithm,", ASME J. Tribology, 112, pp. 42-51.

[15] Brewe, D.E., 1986,"Theoritical Modeling of the Vapor Cavitation in Dynamically Loaded Journal Bearings," ASME J. Tribology, 108, pp. 628-638.

[16] Hirayama, T., Sakurai, T. and Yabe, H. , 2004, " A theoretical Analysis Considering Cavitation Occurrence in Oil-Lubricated Spiral-Grooved Journal Bearings with Experimental Verification," ASME J. Tribology, 126, pp.490-498.

[17] Ikeuchy, K and Mori,H. ,1987,"The effects of Cavity Fluctution on the Elastic and Damping Properties of Journal Bearings," Trans. Jpn. Soc. Mech. Eng.,Ser C, 53(485),pp.136-143 (In Japanese).

[18] Bayada, G., Chambat, M. and El Alaoui, M., 1990," Variational Formulations and Finite Element Algorithms for Cavitation Problems,"ASME, J. Tribology,112, pp. 398-403.

[19] Kumar, A. and Booker, J.F.,1991, " A Finite Element Cavitation Algorithm," ASME J. Tribology, 113,pp. 276-286.

[20] Hajjam, M. and Bonneau, D., 2007 ,"A transient Finite Element Cavitation Algorithm with Application to Radial Lip Seals," Tribology International,40, pp. 1258-1269.

[21] Etsion,L. and Ludwig,L.P., 1982," Observation of Pressure variation in the Cavitation region of submerged Journal bearings," ASME J. Lub. Technology, 104, pp 157-163.

[22] Coyne,J.C. and Elrod, H.G. , 1970 ," Conditions for the rupture of a lubricating film,Part1 :Theoritical model," Trans. ASME, J. Lubric. Techn., pp. 451-456.

[23] Coyne,J.C. and Elrod H.G. , 1971 ," Conditions for the rupture of a lubricating film,Part2 New boundary conditions for Reynolds'equation," Trans. ASME, J. Lubric. Techn., pp. 156-166.

[24] Sun, D.C., Wen, W., Zhiming Z., Xiaoyang, C. and Meili,S.,2008, “Theory of cavitation in an Oscillatory Oil Squeeze film,” Tribology Transactions, 51,pp. 332-340.

[25] Geike, T. and Popov, V., 2009 , “Cavitation within the framework of reduced description of mixed lubrication,’Tribology International, 42, pp.93-98.

[26] Bodeo, S. and Booker, J.F.,1991,” Cavitation in normal separation of square and circular plates,”ASME J. Tribology,” 113,pp 403-410.

[27] Groper, M. and Etsion,I.,2001, ”The effect of shear flow and dissolved Gas diffusion on the cavtation in a submerged journal bearing,” ASME J. Tribology, 123, pp 494-500.

[28] Groper, M. and Etsion,I.,2002, ”Reverse flow as a possible mechanism for cavitation build-up in a submerged journal bearing,” ASME J. Tribology, 124, pp 320-326.

[29] Pan, C.H.T., Kim, T.H. and Rencis, J.J., 2008,” Rolling Stream Trails: An Alternative Cavitation Analysis,” ASME J. Tribology, 130, 021703.

[30] Feng, N.S. and Hahn, E.J. ,1985,” Density and Viscosity Models for Two-phase Homogeneous Hydrodynamic Damper Fluids,” ASLE Transactions, pp. 361-369.

[10] Chamniprasart, K. , Al-Sharif, A., Rajagopal, K.R. and Szeri A.Z. , 1993,”Lubrication With Binary Mixtures: Bubbly oil,”’ ASME J. Tribology, 115, pp. 253-260.

[32] Tao, L., Diaz S., San Andrés, L.S. and Rajagopal K.R., 2000,” Analysis of Squeeze Film Dampers Operating With Bubbly Lubricants,” ASME J. Tribology, 122, pp.205-210.

[33] Diaz, S. and San Andrés, L., 2001, “ A model for Squeeze Film Dampers operating with air Entrainment and Validation with experiments,” ASME J. Tribology, 123, pp.125-133.

[34] Xing, C., Braun, M.J. and Li, H., 2009,” A three Dimensional Navier Stokes Based Numerical Model for Squeeze –Film Dampers . Part1 Effects of Gaseous Cavitation on Pressure Distribution and Damping Coefficients without Consideration of Inertia,” Tribology Transactions,52, pp. 680-694.

[35] Xing, C., Braun, M.J. and Li, H., 2009,” A three Dimensional Navier Stokes Based Numerical Model for Squeeze –Film Dampers . Part 2 Effects of Gaseous Cavitation on the Squeeze Film Dampers,” Tribology Transactions,52, pp. 695-705.

[36] Van Odyck , D.E.A. and Venner, C.H.,2003, “ Compressible Stokes flow in thin film,” A.S.M.E Journal of Tribology , 125, pp. 543-551.

[37] Yang,J, Zhou,L.and Wang,Z.,2011,”Numerical simulation of three-dimensional cavitation around a Hydrofoil,”A.S.M.E. J. Fluids Engineering, 133,081301.

[38] Durany,J., Pereira,J. and Varas,F.,2010,” Dynamical stability of journal-bearing devices through numerical simulation of thermohydrodynamic models,”Tribology International,43, pp.1703-1718

[39] Bresh,D. and Desjardins, B.,2007,"Existence of global weak solutions for a to the Navier Stokes equations for viscous compressible and heat conducting Navier Stokes models," J. Math Pures Appl.,87(4), pp.59-90.

[40] Bair, S.,Khonsari,M.,and Winer,W. O,1998,"High pressure rheology of Lubricants and Limitations of the Reynolds Equation," Tribol. Int.,31(10),pp.573-586.

[41] Chupin,L. and Sart, R.,2012, "Compressible flows: New existence results and justification of the Reynolds asymptotic in thin films," Asymptotic Analysis,76(3-4), pp 193-231.

[42] Fantino R., Frene J. and Godet M., 1972,'"Reynolds equation in viscous film theory,"ASME J. Lub. Technology, 94, pp. 287-288.

[43] Bodeo, S. 2003, "Flow through Rough Microchannels: A lubrication Perspective," First International Conference on Microchannels and Minichannels, Rochester, NY, April 24-25 ,

[44] Coutier-Delgosha,O.,Reboud, J.L. and Delannoy, Y., 2003," Numerical simulation of unsteady cavitating flow," Int. J. for Numerical methods in Fluids, 42(5), pp 527-548.

[45] Pascarella,C., and Salvatore,V.,2001," Numerical Study of Unsteady cavitation on a hydrofoil section using a barotropic model ," 4th Int. Symposium Cavitation, Los Angeles, session B2 .005.

[46] Moreau, J.B., 2005, " Modelisation de l'ecoulement polyphasique a l'interieur et en sortie d'injecteurs diesels, » Thèse, Inst. Nat. Polytechnique de Toulouse, France.

[47] Cristea, A.X., Bouyer,J., Fillon,M. and Pascovici, M.D.,2011, "Pressure and Temperature Fied Measurements of a Lightly Laded Circumferential Groove Journal Bearing," Trib. Trans.,54, pp. 806-823.

[48] Van Wijngaarden,L. 1972,"One dimensional flow of liquid Containing small Gas Bubbles," Annu . Rev . Fluid Mech.,4, pp.369-396.

[49] Mac Adams, W.H., Wood, W.K. and Bryan, R.L. ,1942 ,"Vaporization inside horizontal tubes : Benzene-Oil mixtures," Trans. ASME, 64,pp. 193.

[50] Hayward, A.T.J. ,1961,"The viscosity of bubbly oil," National Eng. Lab. ,Glasgow, U.K. , Fluids Report 99.

[51] Wallis,G.B.,1969, One dimensional two-phase flow. Mc Graw Hill

[52] Kubota, A., Kato,H., and Yamaguchi,H.,1992, "A new Modeling of cavitation flows: A numerical study of unsteady Cavitation on a Hydrofoil," J. Fluid Mech.,240, pp. 59-96.

[53] Migout, Fabien, "Etude théorique et expérimentale du changement de phase dans l'interface des garnitures mécaniques d'étanchéité, " Thèse, Université de Poitiers, Décembre 2010.

[54]Song H.S. ,Klaus E.E. and Duda J.L., 1991, "Prediction of bulk modulus values for fluids and lubricants," Journal Basic Engineering, 86(3), pp.469-473.

[55] Sahlin,F., Almquist, A., Larsson, R.and Glavatskih,S., 2007, “A cavitation algorithm for arbitrary lubricant compressibility,” Tribology International ,40, pp.1294-1300.

[56] Dowson, D. and Higginson, G.R., 1966, Elasto Hydro-dynamic lubrication, Oxford.

[57] Dellanoy,Y and Kueny,J.L., 1990, “Two phase flow approach in unsteady cavitation modeling,”98, ASME FED *Cavitation and Multiphase flow forum*, pp.153-158.

[58] Hoeijmakers, H.W.M., Jansens, M.E., and Kwan, W. ,1998, “Numerical simulation of sheet cavitation,” *Proceedings of the third International Congress on Cavitation*, Grenoble, France.

[59] Sobahan, Mia,”Prediction of Tribological and Rheological Properties of Lubricating Oils by Sound Velocity,” Phd Thesis, School of Science and Engineering, Saga University , Japan , Sept. 2010.

[60] Ausas,R., Ragot,P., Leiva, J.,Jai, M.,Bayada,G. and Buscaglia, G.C., 2007,“ The impact of the cavitation model in the analysis of a microtextured lubricated journal bearings,”Journal of Tribology,129(3), pp 868-875

[61] Etsion,I. and Pinkus,O., 1974,“Analysis of short journal bearings with new upstream boundary conditions,” ASME J. Lub. Tech. 96, pp 489-496.

[62] Etsion,I. and Pinkus,O., 1975,“Solutions of finite journal bearings with incomplete films,” ASME J. Lub. Tech., 97,pp 89-93.

[63] Vincent,B., Maspeyrot, P. and Frêne, J.,1995,“Starvation and cavitation effects in finite journal bearings,” Leeds Lyon Symposium, Lubricants and Lubrification, D. Dowson and al (editors), Elsevier Science Tribology series 30, pp 455-464. .

[64] Liu,S.,2012, “On boundary conditions in lubrication with one dimensional analytical solutions,” Tribology International ,48, pp.182-190.

[65] Ausas, R, Jai, M.and Buscaglia, G. C. ,2009, “A mass-conserving algorithm for dynamical lubrication problems with cavitation,” Journal of Tribology, 131, 031702-1.

Nomenclature

c_v,c_l ,c_f velocity of the sound in the pure vapour, pure liquid , mixture regime
c_{min} parameter in the pressure-density law
h (H) gap (non dimensional)
l characteristic length
h (H) gap (non dimensional)
p (p*) pressure (non dimensional)
r_c, r_ρ, r_η ratio of velocity, density and viscosity for pure vapour/pure liquid values

x (X) coordinate (non dimensional)
u (S) velocity component in the x-direction (non dimensional)
C_1, C_2, C_3 parameters in the pressure-density law
F friction force
Q mass flow
L_1,L_2 characteristic lengths
L_{11},L_{12},L_{13},L_{31},L_{32} geometrical parameters for the bearing
M mass volume fraction of the vapor
P_{ext} boundary pressure
P_{vm}, (P_{ml} =P_{sat}) wet point pressure, (bubble point pressure)
P_{cav} "cavitation pressure" for JFO- E. A. models
R non dimensional number
U (S) velocity vector (non dimensional)
V characteristic value of the velocity
W load
α volume fraction of the vapor (generalized following equation(8b))
β bulk modulus in the Elrod-Adams model
μ, μ_l, μ_v viscosity, viscosity of the liquid phase, viscosity of the vapour phase
ρ, ρ_l , ρ_v density, density of the liquid phase, density of the vapour phase
ρ_c density parameter in the Elrod Adams model
ρ^* non dimensional density
λ auxiliary function in the Navier Stokes equation (second Lamé coefficient)
θ relative density ($\theta = \rho/\rho_l$) (also called relative saturation)

Figure captions

Fig 1 : example of geometry
Fig.2 :Saturation pressure laws A comparison between cavitation models. Low pressure
Fig.3 :Saturation pressure laws A comparison between cavitation models. High pressure
Fig 4 Model gap (sections 4-5-6)
Fig.5 : A comparison between models. Pressure curves
Fig.6 : A comparison between models. Relative density curves
Fig.7: Dukler mixture viscosity model. Influence of r_ρ ratio. Pressure curves
Fig.8 : Dukler mixture viscosity model. Influence of r_ρ ratio. Relative density curves
Fig 9: Light loading. Influence of cavitation parameters. Comparison between various models. Relative density curves.
Fig 10: Light loading. Influence of cavitation parameters. Comparison between various models. Pressure curves
Fig 11 Model gap (sections 7-8)
Fig 12 : Starved situation. A comparison between various models. Pressure curves
Fig 13 : A comparison of the pressure field (finite bearing): Experimental values (top) present model (middle) and JFO model (bottom). Pressure values in Mpa.

Table captions

Table 1: Comparison between various models: Values of operational parameters
Table 2: Value of mixture-liquid transition pressure. Influence of internal parameters
Table 3 : Load and minimal saturation values as a function of r_c and r_ρ
(Dukler model $r_\mu=10^{-2}$, 10^{-3},10^{-4},10^{-5}, Mc Adams model , $r_\mu =10^{-2}$)

Table 4 : Load and minimal saturation values as a function of r_ρ and r_c.
(Mc Adams model , $r_\mu = 10^{-4}$)
Table 5 : Load and minimal saturation values as a function of r_ρ and r_c..
(Mc Adams model , $r_\mu = 10^{-5}$)
Table 6: Comparison between various models: Values of operational parameters. Fully flooded situation
Table 7: Comparison between various models: Values of operational parameters. Starved situation
Table 8: Light loading. Influence of cavitation parameters: Values of operational parameters for E. A. model
Table 9: Light loading. Influence of cavitation parameters: Values of operational parameters New model.

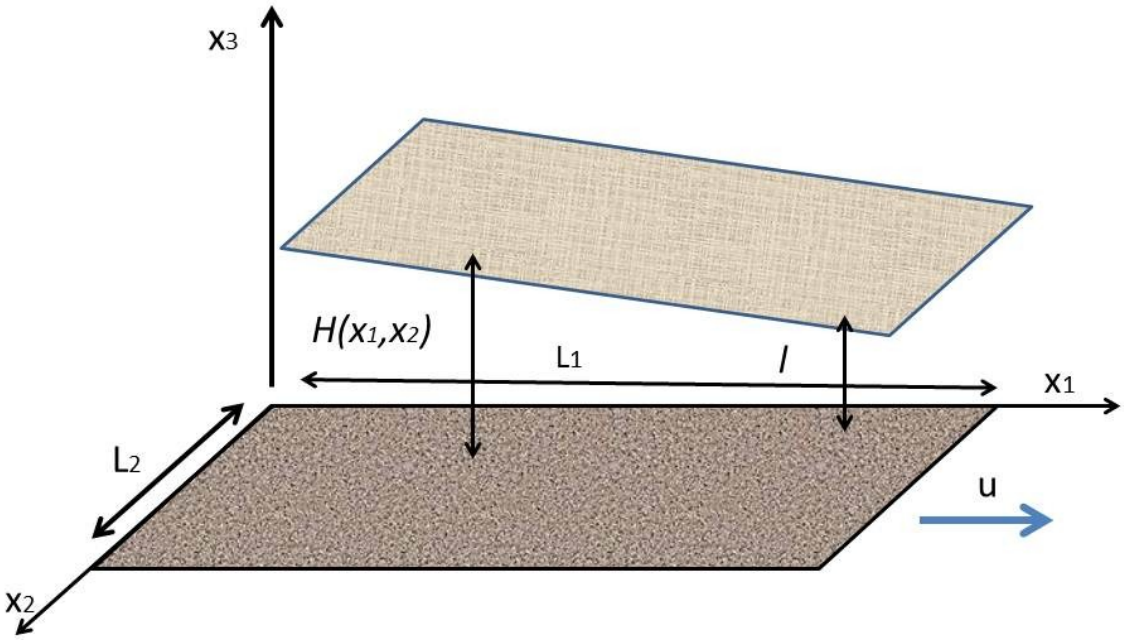

Figure 1: example of geometry.

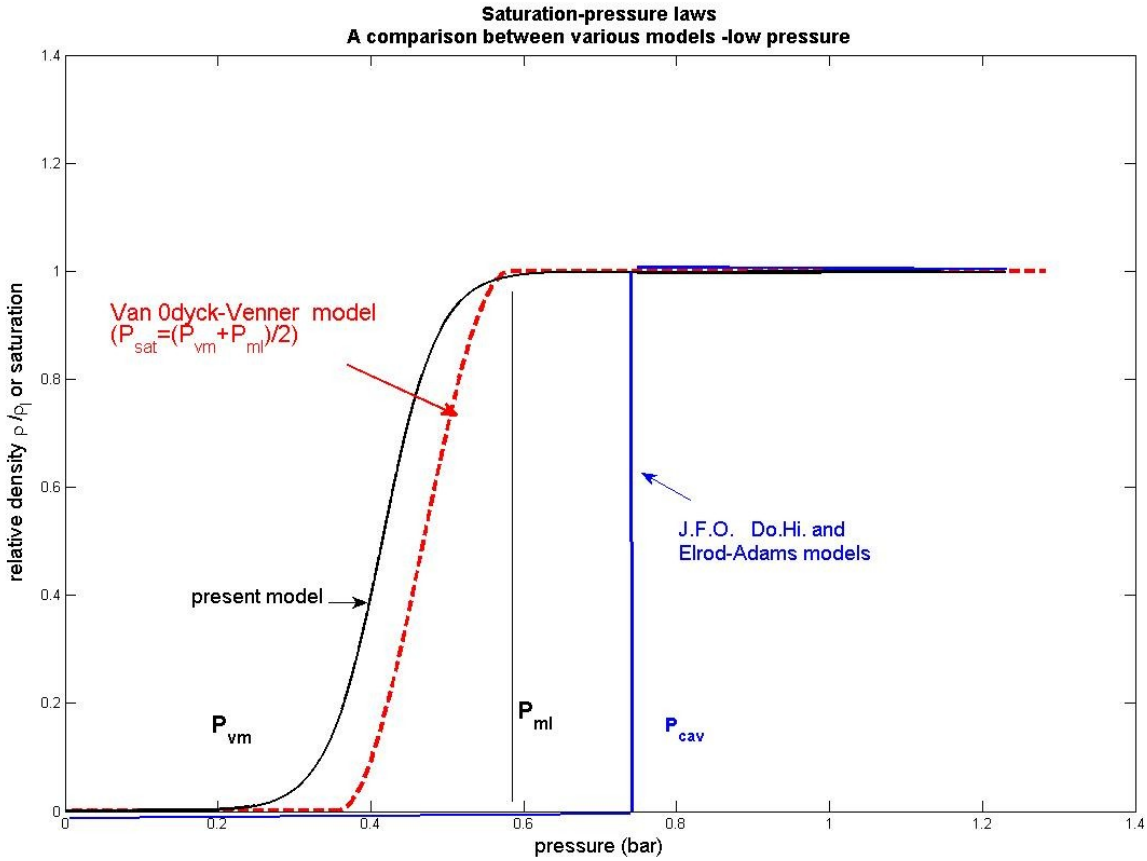

Figure 2: Saturation pressure laws A comparison between models. Low pressure.

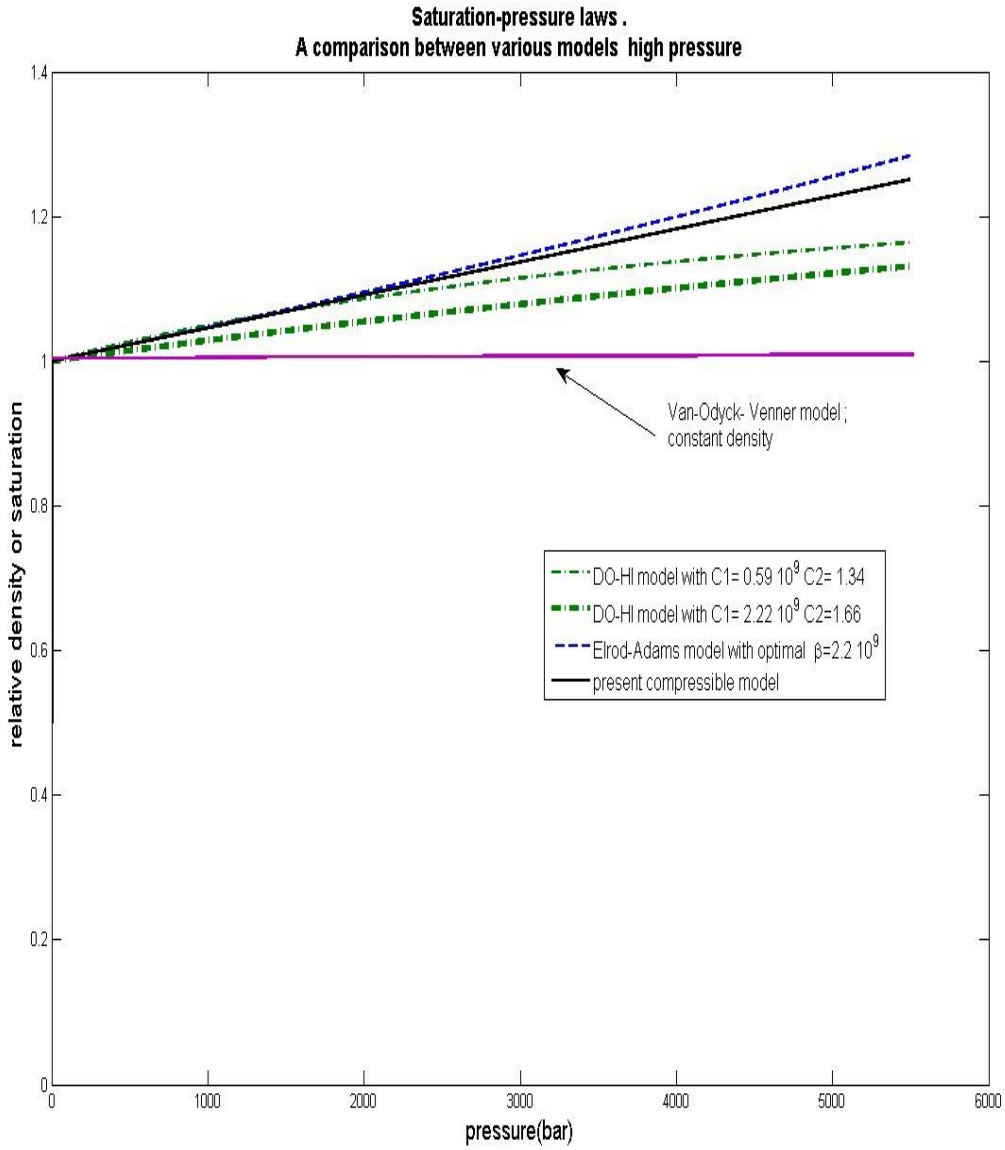

Figure 3: Saturation pressure laws A comparison between models. High pressure.

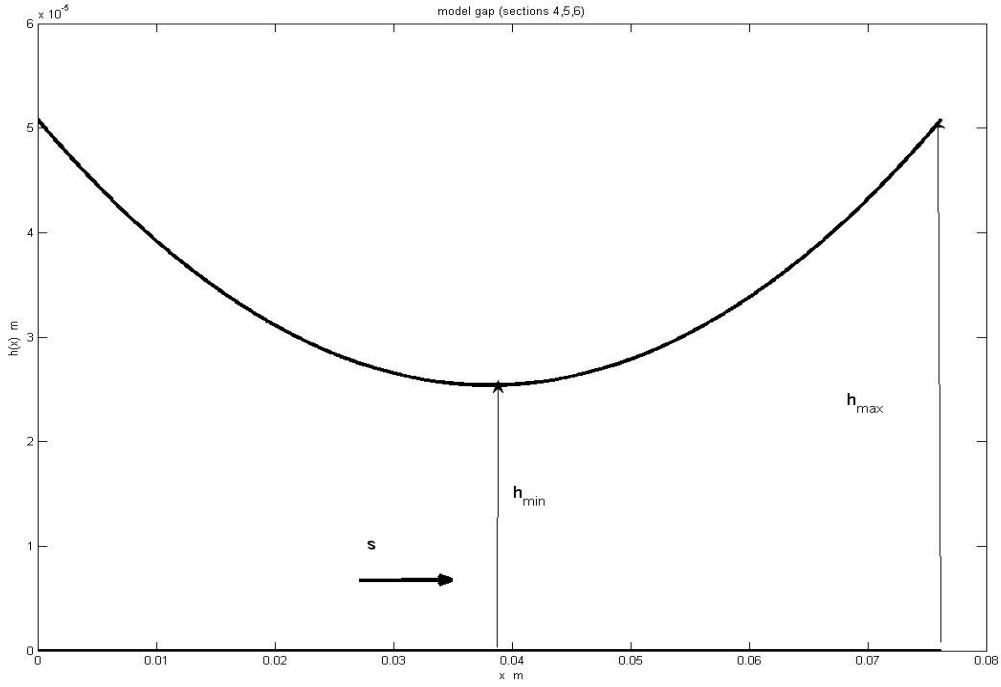

Figure 4: Model gap.

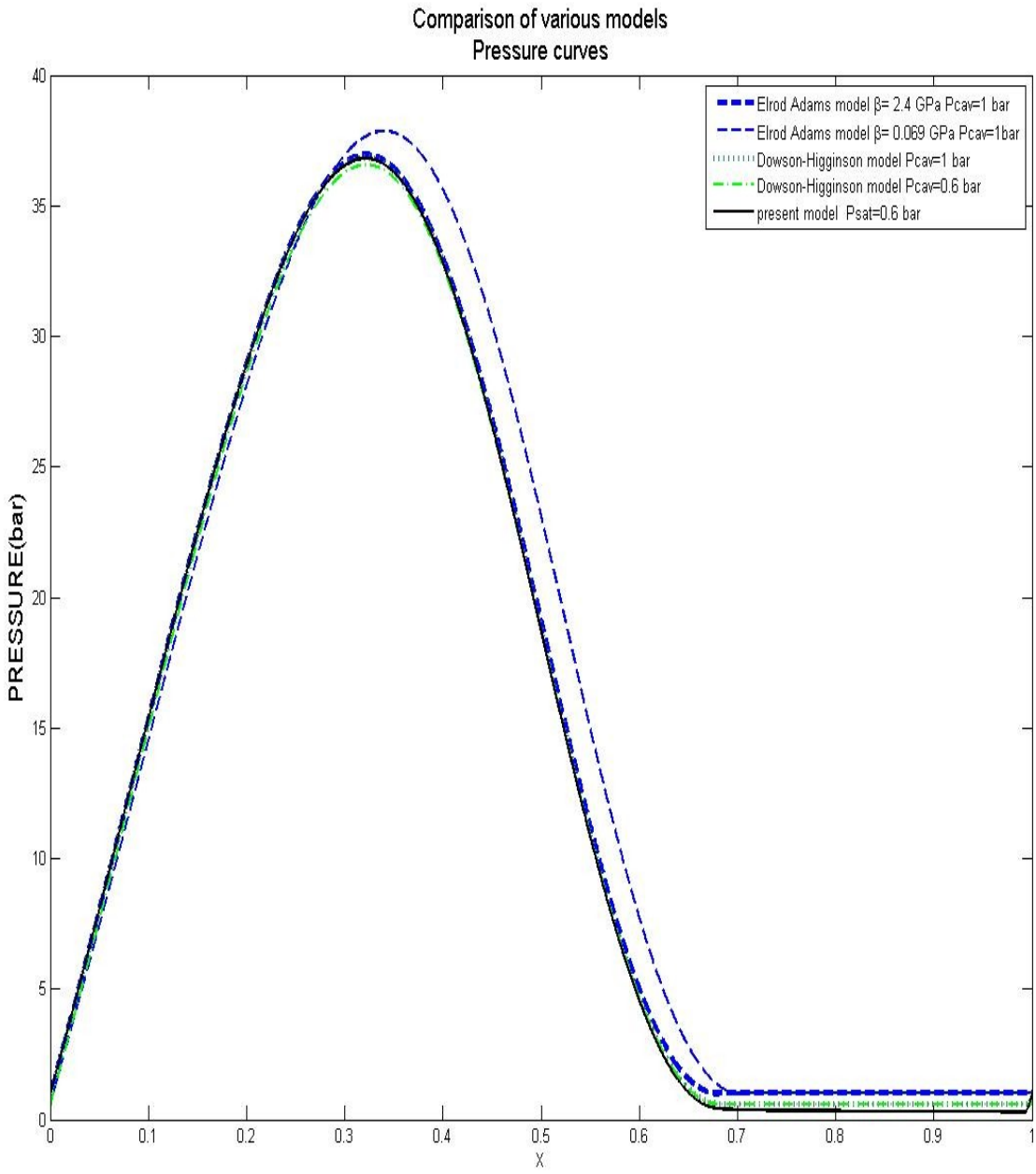

Figure5 : A comparison between models: Pressure curves.

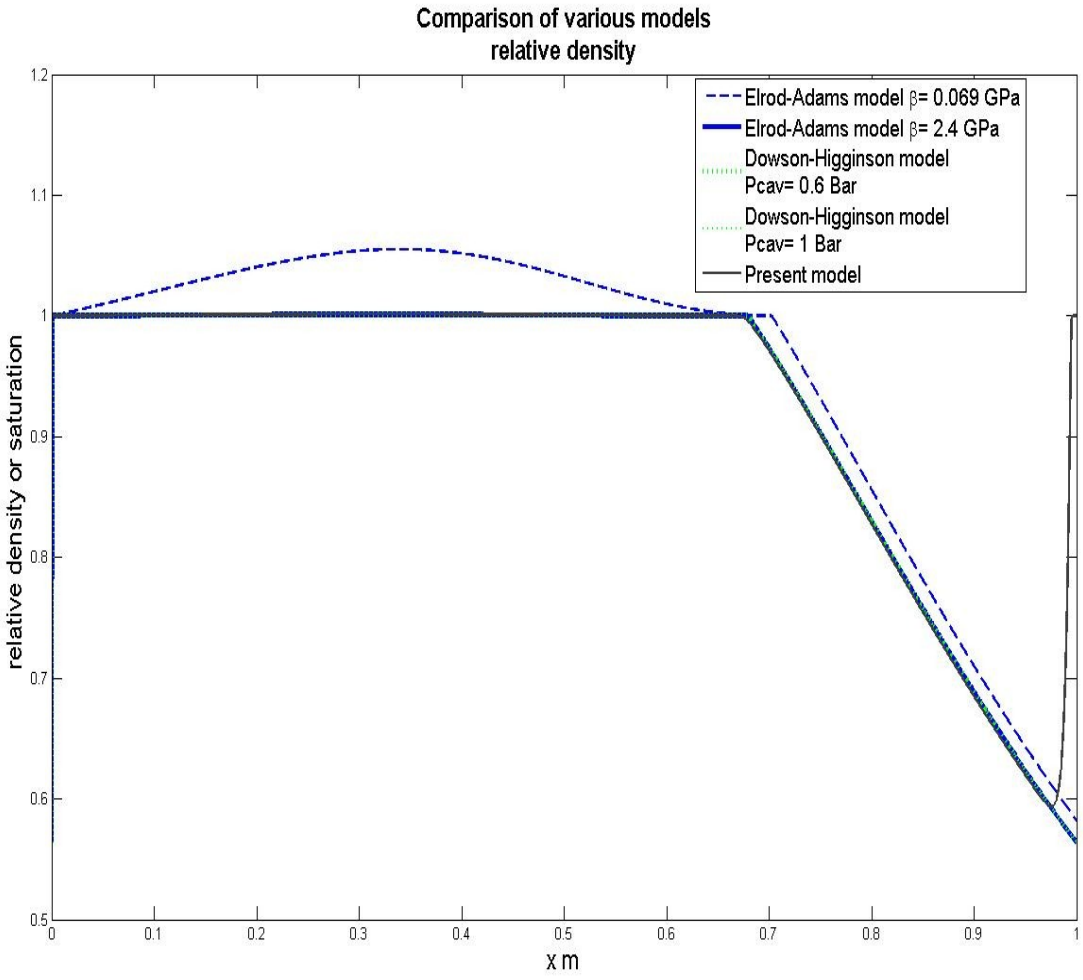

Figure 6: A comparison between models. Saturation curves.

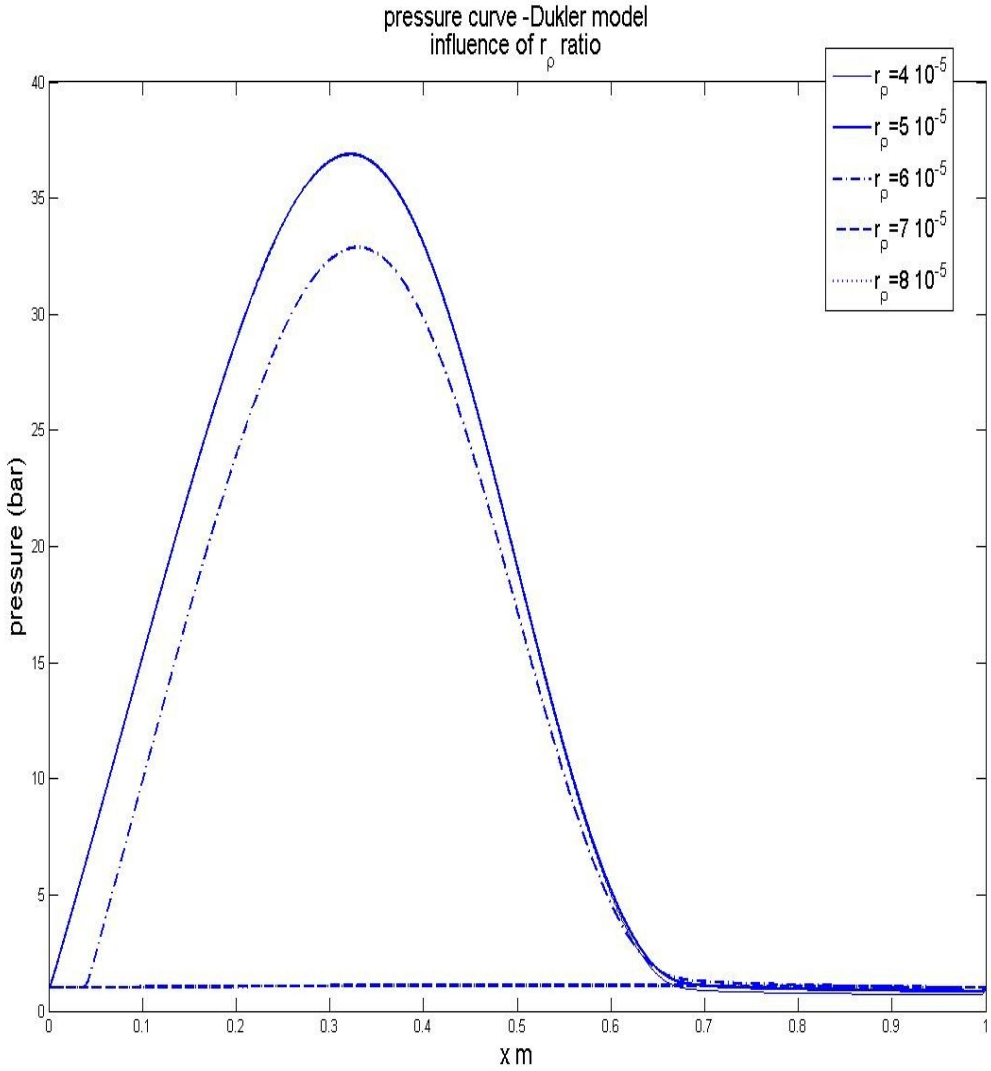

Figure 7 : Dukler mixture viscosity model . Influence of r_ρ ratio. Pressure curves.

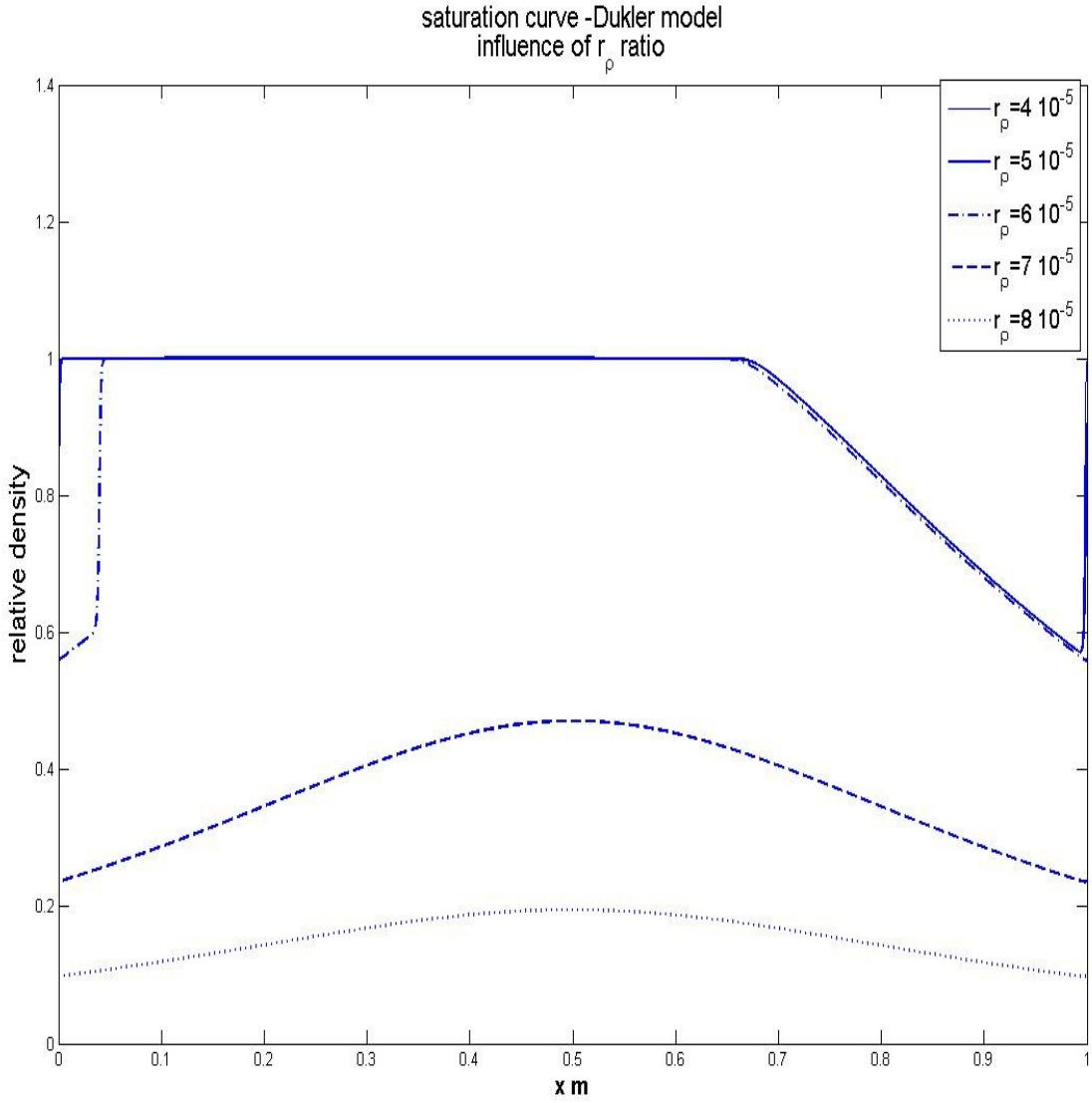

Figure 8: Dukler mixture viscosity model. Influence of r_ρ ratio. Saturation curves.

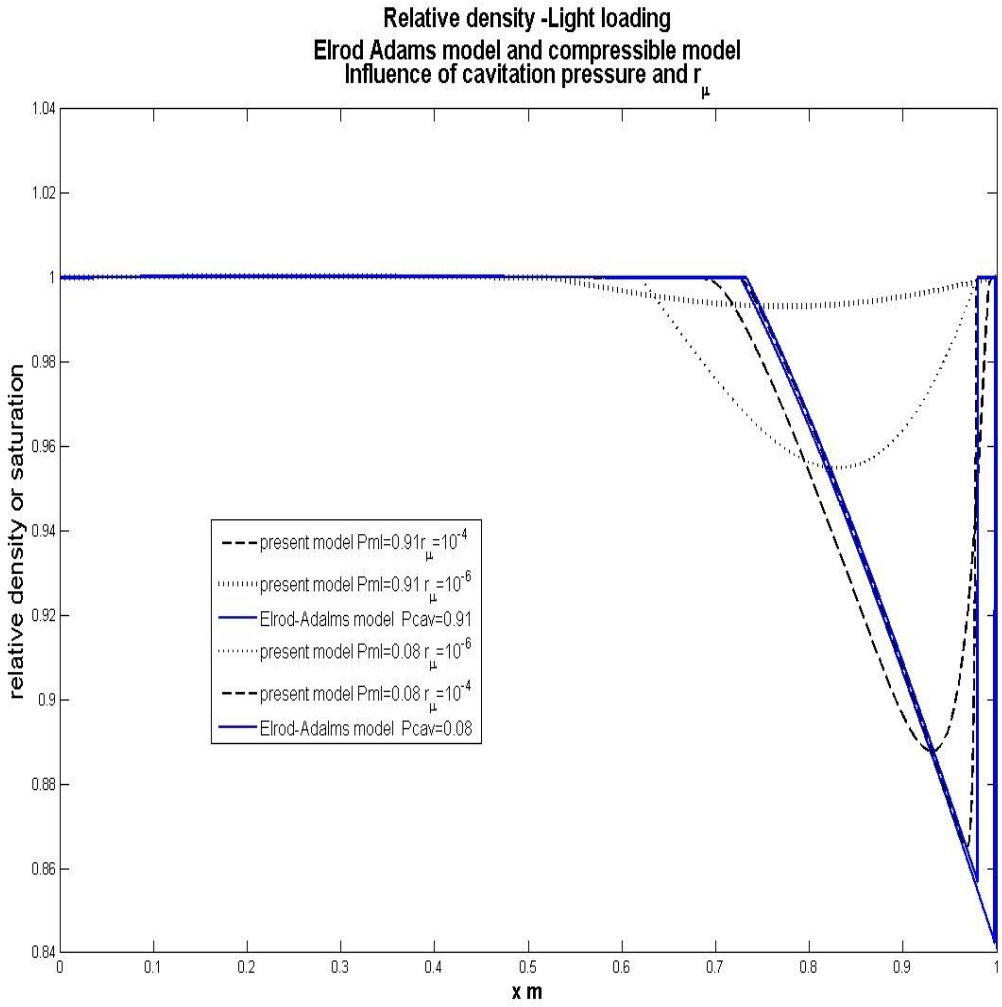

Figure 9: Light loading. Influence of cavitation parameters . Comparison between various models. Saturation curves.

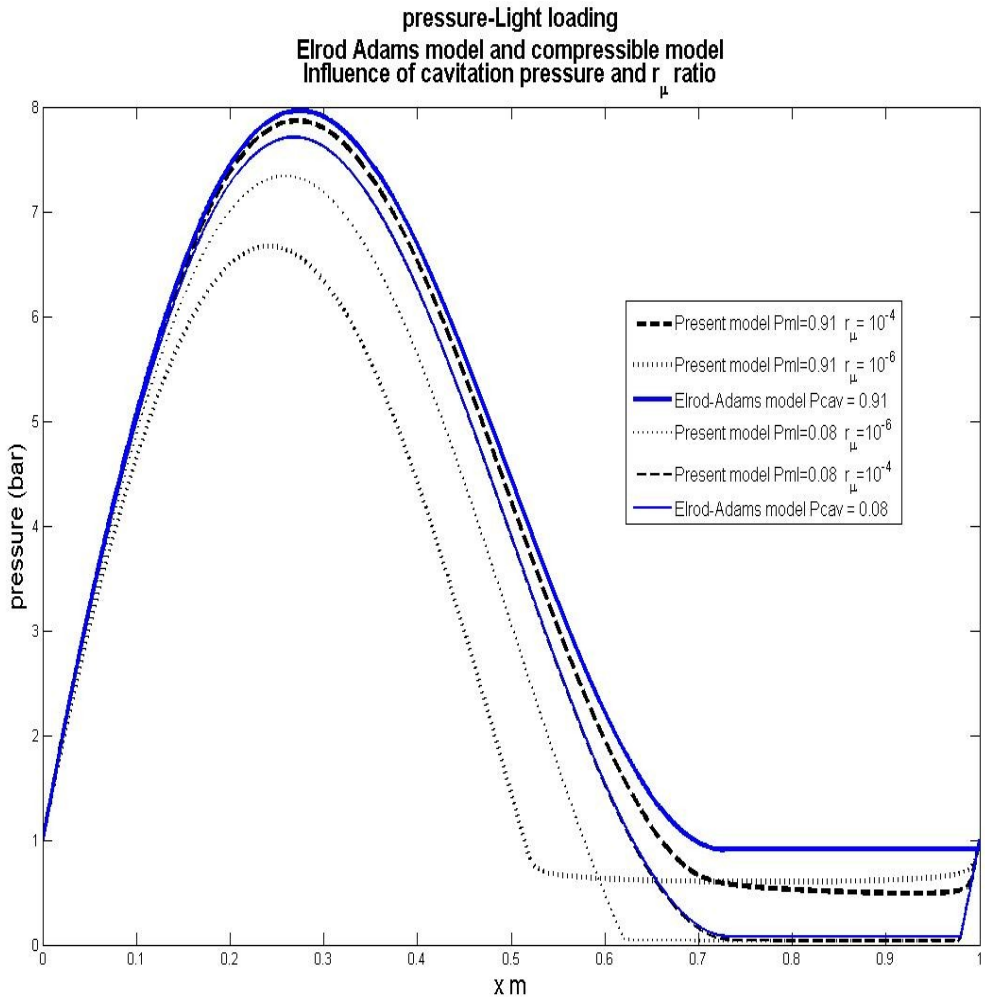

Figure 10: Light loading. Influence of cavitation parameters. Comparison between various models. Pressure curves.

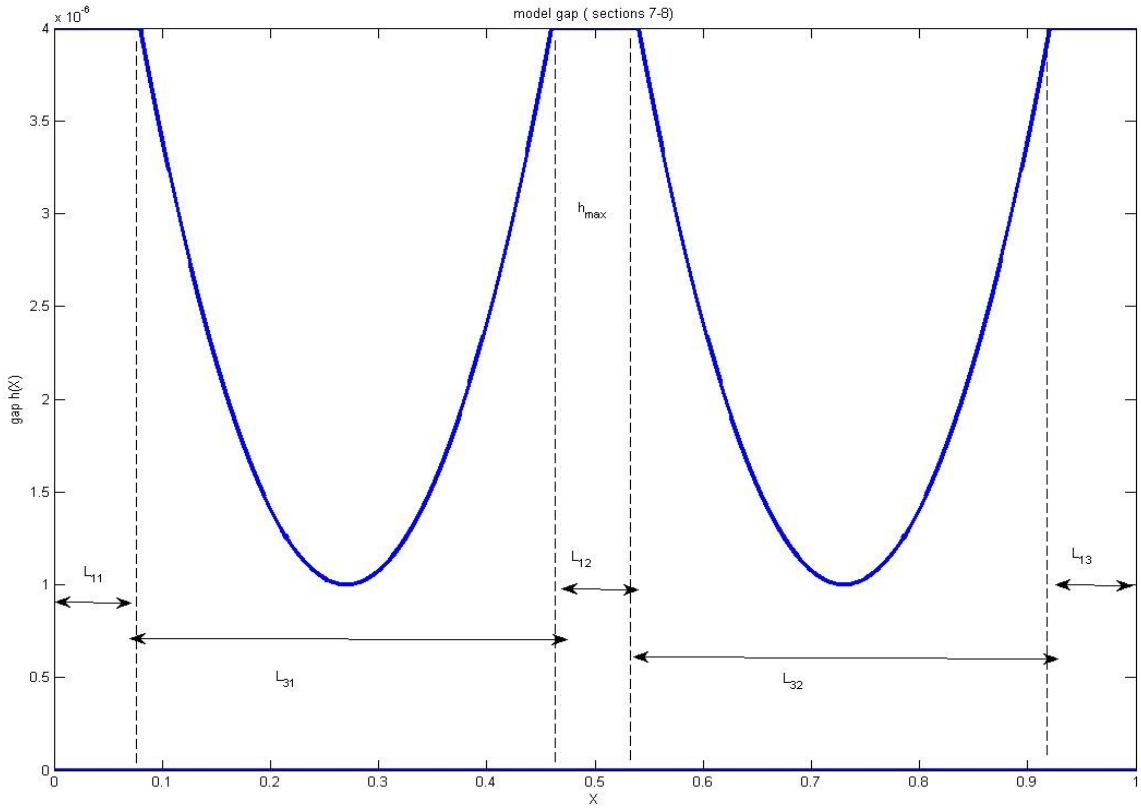

Figure 11: Double slider geometry.

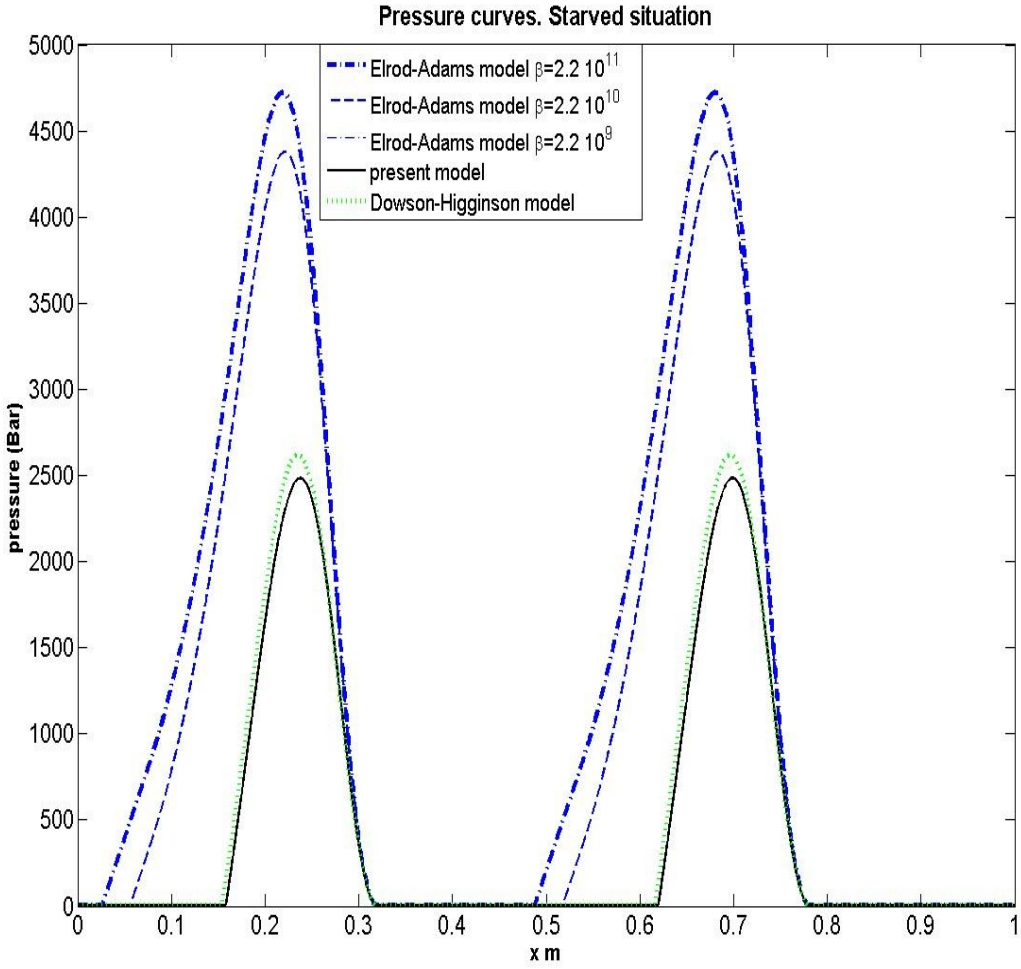

Figure 12: Starved situation. A comparison between various models. Pressure curves .

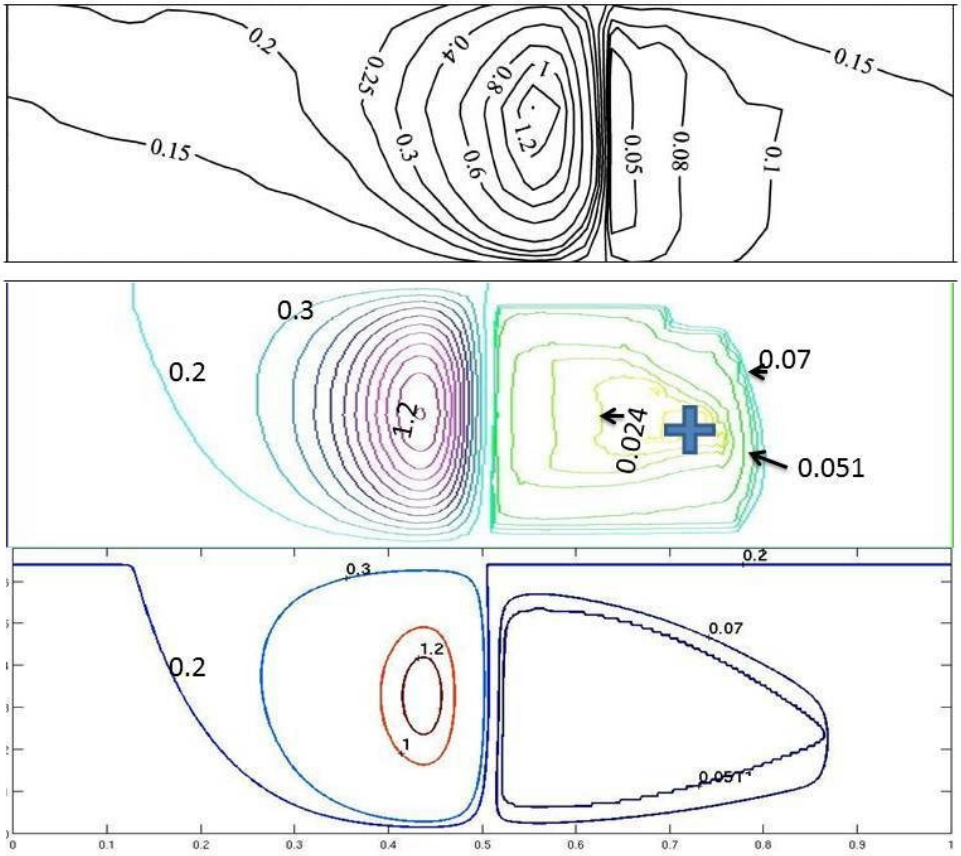

Figure 13: A comparison of the pressure field (finite bearing): Experimental values (top) present model (middle) and J.F.O. model (bottom). Pressure values in Mpa.

model	Load (N/m)	Maximum pressure (10^5 Pa)	Minimum saturation	Flow (m^2/s)	Friction (N/m)
E.A. β=0.069 GPa Pcav=10^5 Pa	1.00 10^5	38	0.58	6.8 10^{-5}	445/337
E.A. β=2.4 GPa Pcav=10^5 Pa	0.92 10^5	37	0.57	6.5 10^{-5}	445/327
Do.Hi. Pcav=10^5 Pa	0.93 10^5	36.9	0.56	6.55 10^{-5}	445/327
Do.Hi. Pcav=0.6$10^5$ Pa	0.90 10^5	36.5	0.56	6.5 10^{-5}	445/327
Present model	0.90 10^5	36.8	0.58	6.5 10^{-5}	445

Table 1: Comparison between various models: Values of operational parameters.

Load (Newton/m) /minimal saturation	r_ρ = 4 10^{-5}	r_ρ =5 10^{-5}	r_ρ = 6 10^{-5}	r_ρ = 7 10^{-5}	r_ρ = 8 10^{-5}
r_c =0.05	0.90 10^5 /0.57	0.89 10^5 /0.57	0.89 10^5 /0.57	0.89 10^5 /0.57	0.89 10^5 /0.57
r_c =0.1	0.90 10^5 /0.57	0.90 10^5 /0.57	0.90 10^5 /0.57	0.90 10^5 /0.57	0.90 10^5 /0.57
r_c =0.22	1.02 10^5 /0.57	1.02 10^5 /0.57	1.02 10^5 /0.57	1.02 10^5 /0.57	1.02 10^5 /0.57
r_c =0.225	1.02 10^5 /0.57	1.02 10^5 /0.57	1.02 10^5 /0.57	1.02 10^5 /0.57	0.02 10^5/0.43
r_c =0.25	1.02 10^5 /0.57	1.02 10^5 /0.57	0.77.10^5 /0.56	0.02.10^5 /0.23	0.02.10^5 /0.1

Table 2: Load and minimal saturation values as a function of r_ρ and r_c (Dukler model r_μ =10^{-2}, 10^{-3},10^{-4},10^{-5}, Mc Adams model , r_μ =10^{-2}).

Load(N/m)/minimal saturation	r_ρ = 4 10^{-5}	r_ρ =5 10^{-5}	r_ρ = 6 10^{-5}	r_ρ = 7 10^{-5}	r_ρ = 8 10^{-5}
r_c =0.05	0.89 10^5 /0.61	0.90 10^5 /0.62	0.90 10^5 /0.63	0.90 10^5 /0.65	0.90 10^5 /0.66
r_c =0.01	0.89 10^5 /0.61	0.90 10^5 /0.62	0.90 10^5 /0.63	0.90 10^5 /0.65	0.90 10^5 /0.66
r_c =0.22	1.02 10^5 /0.66	0.92 10^5 /0.69	0.90 10^5 /0.71	0.71 10^5 /0.69	0.02 10^5 /0.52
r_c =0.225	0.92 10^5 /0.66	0.92 10^5 /0.69	0.89 10^5 /0.71	0.54 10^5 /0.67	0.02 10^5 /0.42
r_c =0.25	0.92 10^5 /0.68	0.86 10^5 /0.69	0.02 10^5 /0.53	0.02 10^5 /0.23	0.02 10^5 /0.1

Table 3 : Load and minimal saturation values as a function of r_ρ and r_c. (Mc Adams model, r_μ =10^{-4}).

Load (N/m) /minimal saturation	$r_\rho = 4\ 10^{-5}$	$r_\rho = 5\ 10^{-5}$	$r_\rho = 6\ 10^{-5}$	$r_\rho = 7\ 10^{-5}$	$r_\rho = 8\ 10^{-5}$
$r_c = 0.05$	$0.89\ 10^5$ /0.64	$0.89\ 10^5$ /0.66	$0.89\ 10^5$ /0.68	0.8910^5 /0.69	$0.89\ 10^5$ /0.71
$r_c = 0.1$	$0.89\ 10^5$ /0.71	$0.88\ 10^5$ /0.74	$0.87\ 10^5$ /0.78	$0.86\ 10^5$ /0.80	$0.84\ 10^5$ /0.82
$r_c = 0.22$	$0.84\ 10^5$ /0.83	$0.79\ 10^5$ /0.87	$0.57\ 10^5$ /0.88	$0.02\ 10^5$ /0.78	$0.02\ 10^5$ /0.53
$r_c = 0.225$	$0.84\ 10^5$ /0.84	$0.79\ 10^5$ /0.87	$0.39\ 10^5$ /0.86	$0.02\ 10^5$ /0.70	$0.02\ 10^5$ /0.42
$r_c = 0.25$	$0.80\ 10^5$ /0.85	$0.24\ 10^5$ /0.83	$0.02\ 10^5$ /0.54	$0.02\ 10^5$ /0.23	$0.02\ 10^5$ /0.1

Table 4 : Load and minimal saturation values as a function of r_ρ and r_c (Mc Adams model, $r_\mu = 10^{-5}$).

P_{ml} (bar)	$r_\rho = 4\ 10^{-5}$	$r_\rho = 5\ 10^{-5}$	$r_\rho = 6\ 10^{-5}$	$r_\rho = 7\ 10^{-5}$	$r_\rho = 8\ 10^{-5}$
$r_c = 0.05$	0.07	0.08	0.1	0.11	0.12
r_c l=0.1	0.25	0.31	0.36	0.42	0.48
$r_c = 0.22$	0.95	1.17	1.38	1.59	1.79
$r_c = 0.225$	1.19	1.46	1.73	1.99	2.25
$r_c = 0.25$	1.46	1.79	2.12	2.44	2.75

Table 5: Value of mixture-liquid transition pressure. Influence of internal parameters.

P_{cav} =0.08bar	P_{cav} = 0.37 bar	P_{cav} =0.91 bar
W=7.21 Pmax=7.71 θ_{min}=0.84	W=7.75 Pmax=7.80 θ_{min}=0.84	W=8.77 Pmax=7.96 θ_{min}=0.86

Table 6: Light loading. Influence of cavitation parameters: Values of operational parameters load W (n/m) , maximum pressure (Bar), and minimal saturation for E. A. model.

	P_{cav} =0.08 Dukler model	P_{cav} =0.08 Mc Adams model	P_{cav} =0.37 Dukler model	P_{cav} = 0.37 Mc Adams model	P_{cav} =0.91 Dukler model	P_{cav} =0.91 Mc Adams model
$r_\mu = 10^{-4}$	W=7.16 Pmax=7.71 Pmin=0.036 θ_{min}=0.86	W=7.16 Pmax=7.71 Pmin=0.036 θ_{min}=0.86	W=7.50 Pmax=7.77 Pmin=0.18 θ_{min}=0.86	W=7.48 Pmax=7.6 Pmin=0.19 θ_{min}=0.88	W=8.16 Pmax=7.88 Pmin=0.48 θ_{min}=0.85	W=8.10 Pmax=7.88 Pmin=0.49 θ_{min}=0.89
$r_\mu = 10^{-5}$	W=7.16 Pmax=7.71 Pmin=0.036 θ_{min}=0.86	W=7.13 Pmax=7.70 Pmin=0.036 θ_{min}=0.89	W=7.50 Pmax=7.77 Pmin=0.18 θ_{min}=0.86	W=.6.71 Pmax=7.51 Pmin=0.20 θ_{min}=0.94	W=8.16 Pmax=7.88 Pmin=0.48 θ_{min}=0.85	W=6.89 Pmax=7.42 Pmin=0.53 θ_{min}=0.95
$r_\mu = 10^{-6}$	W=7.16 Pmax=7.71 Pmin=0.036 θ_{min}=0.86	W=6.08 Pmax=7.34 Pmin=0.039 θ_{min}=0.95	W=7.50 Pmax=7.77 Pmin=0.18 θ_{min}=0.86	W=4.90 Pmax=6.73 Pmin=0.23 θ_{min}=0.99	W=8.16 Pmax=7.88 Pmin=0.48 θ_{min}=0.85	W=5.34 Pmax=6.67 Pmin=0.60 θ_{min}=0.99

Table 7: Light loading. Influence of cavitation parameters: Values of operational parameters load W (n/m) , maximum and minimum pressure (Bar), and minimal saturation. New model.

model	Load (N/m)	Max pressure GPa	Minimum density	Flow rate (m^2/s)	Friction N/m	Percentage of non cavitated area
E.A β= 0.22 GPa	139 10^6	0.256	0.80	12.8 10^{-6}	3463/3249	0.84
E.A. β= 2.2 GPa	218 10^6	0.539	0.36	5.71 10^{-6}	4062/3293	0.68
E.A β= 22 GPa	197 10^6	0.509	0.31	4.94 10^{-6}	4103 /3157	0.64
E.A. β=220 GPa	194 10^6	0.505	0.31	4.88 10^{-6}	4103 /3140	0.64
Present model	217 10^6	0.539	0.35	5.66 10^{-6}	4069	0.68
Do.Hi. model	210 10^6	0.530	0.33	5.41 10^{-6}	4089/3260	0.67

Table 8: Comparison between various models: Values of operational parameters. Fully flooded situation.

model	Load (N/m)	Max pressure GPA	Minimum density	Flow rate (m^2/s)	Friction (N/m)	Percentage of non cavitated area
E.A. β= 2.2 10^9	57 10^6	0.249	0.30	4.84 10^{-6}	3386/2109	0.32
E.A β= 2.2 10^{10}	146 10^6	0.437	0.30	4.84 10^{-6}	3850/2788	0.53
E.A. β= 2.2 10^{11}	168 10^6	0.474	0.30	4.84 10^{-6}	3987 /2972	0.59
Present model	57 10^6	0.248	0.30	4.84 10^{-6}	3386	0.32
Do.Hi. model	61 10^6	0.261	0.30	4.84 10^{-6}	3403/1851	0.33

Table 9: Comparison between various models: Values of operational parameters. Starved situation.